

# Two Slot Array with Near Zero Refractive Index Substrate

Student Name: Namrata Singh

IIIT-D MTech ECE

July, 2015

Under the Supervision of Dr. Shobha Sundar Ram

Indraprastha Institute of Information Technology Delhi

July, 2015

# Two Slot Array with Near Zero Refractive Index Substrate

Student Name: Namrata Singh

IIIT-D MTech ECE

July, 2015

Indraprastha Institute of Information Technology  
New Delhi

Submitted in partial fulfillment of the requirements  
for the Degree of Master of Technology in Electronics and Communication

## Certificate

This is to certify that the thesis titled “**Two Slot Array with Near Zero Refractive Index Substrate**” being submitted by Namrata Singh to the Indraprastha Institute of Information Technology Delhi, for the award of the *Master of Technology in Electronics and Communication Engineering*, is an original research work carried out by her under my guidance and supervision. In my opinion, the thesis has reached the standards fulfilling the requirements of the regulations relating to the degree.

The results contained in this thesis have not been submitted in part or full to any other university or institute for the award of any degree/diploma.

**July, 2015**

**Dr.Shobha Sundar Ram**  
**Department of Electronics and Communication**  
**Indraprastha Institute of Information Technology Delhi**  
**New Delhi, 110020**

## Acknowledgement

I appreciate the help of many people for supporting and assisting my Thesis study.

I am grateful to **Dr. Shobha Sundar Ram** for being an extraordinary advisor who was always there to guide me at difficult stages of research. Her enthusiasm, encouragement and faith in me throughout have been extremely helpful. I sincerely thank her for being my advisor for this period and for helping me positively with her vast knowledge.

I am thankful to my parents, husband, siblings and friends who have always encouraged me to achieve my goals and pursuits and without their help and emotional support all this would have not been possible. I would like to thank them from the bottom of my heart for all their support and concerns in everything over this year.

I thank IIIT Delhi for providing an enthusiastic and peaceful atmosphere, well facilitated ECE lab to carry on work uninterrupted.

**Namrata Singh**  
**MT13157**

## Abstract

Highly directive antennas are useful in applications such as satellite communications, radar systems and biomedical applications. Directivity is usually achieved using either large antenna apertures or array systems comprising many antenna elements. In recent times, metamaterials have been investigated for improving the directivity of different types of antennas such as linear wire antennas, patch antennas, horn antennas, slot antennas etc.

In this work, we investigate the possibility of improving the directivity of a slot antenna with a metamaterial substrate and a source excitation within the substrate. The metamaterial substrate is modelled as a Debye medium with dispersive permittivity and permeability. The refractive index of the substrate is (a) negative at frequencies below the plasma frequency, (b) zero at the plasma frequency, (c) positive at frequencies above the plasma frequency.

We demonstrate a directive 3D (three-dimensional) two-slot antenna structure with a near zero refractive index substrate that is capable of directing the main lobe of the radiation away from the broadside based on the position of the source within the substrate, with respect to the two slot apertures. The effect of antenna parameters, such as material of the substrate, length of the aperture or slot length, width of the slot, spacing between the slots, height of the substrate and the choice of plasma frequency of the metamaterial, on the far-field radiation pattern and directivity of the antenna are studied.

Transverse magnetic (TM) mode wave propagation is simulated using the finite difference time domain (FDTD) techniques with perfectly matched boundary conditions. The far-field radiation pattern of the 3D two-slot antenna is estimated from the electric fields at the aperture. The results indicate that reduced beam width is achieved for a bandwidth of frequencies around the plasma frequency when compared to a conventional slot antenna with the air substrate. These results imply that 3D two-slot antenna design could be extended to 3D multi-slot antenna design for better directivity and controllability in beam steering.

# Contents

<b>1</b>	<b>Introduction</b>	<b>1</b>
1.1	Organization of Thesis . . . . .	2
1.2	Metamaterial concepts . . . . .	2
1.3	History of metamaterials for design of directive antennas . . . . .	3
1.4	Problem Statement and Objectives . . . . .	9
<b>2</b>	<b>Simulation Modeling</b>	<b>10</b>
2.1	Derivation of three dimensional (3D) FDTD equations . . . . .	11
2.2	Derivation of far field equations of an aperture antenna from near field equations	14
<b>3</b>	<b>Results</b>	<b>18</b>
3.1	Results for far-field radiation pattern for 2D two-slot antenna design: . . . . .	19
3.2	Results for far-field radiation pattern for 3D two-slot antenna design: . . . . .	21
3.2.1	Case (I) . . . . .	21
3.2.2	Case (II) . . . . .	23
3.2.3	Case (III) . . . . .	23
3.2.4	Case (IV) . . . . .	24
3.2.5	Case (V) . . . . .	26
3.2.6	Case (VI) . . . . .	26
3.2.7	Case (VII) . . . . .	28
3.2.8	Case (VIII) . . . . .	30
<b>4</b>	<b>Conclusion and Future Work</b>	<b>33</b>
4.1	Conclusion . . . . .	33
4.2	Future Work . . . . .	34

# List of Figures

1.1	Different combinations of $\epsilon$ and $\mu$ and type of wave propagation in that medium	3
1.2	2-D FDTD simulation of wave propagation in metamaterial [3]. The source is kept outside the metamaterial medium. . . . .	4
1.3	Comparison of the electric field generated by an infinite current sheet driven by a 30 GHz source in a matched zero-index Drude medium slab and in free-space .	5
1.4	Different refraction scenarios when rays travel from metamaterial to free space medium. . . . .	5
2.1	3D Problem Structure top-view and side-view . . . . .	10
2.2	Structure of the Yee cell located at (i,j,k). 6 field components ( $E_x, E_y, E_z, H_x, H_y, H_z$ ) are arranged around (i,j,k) with half grid differences satisfying the Maxwell's equations. (x), (y), (z) is the axis considered for problem formulation. . . . .	12
2.3	Geometry used for the far-field computation [11] . . . . .	15
2.4	Diagram to explain Surface Equivalence Theorem . . . . .	16
2.5	Pictorial representation of aperture placed in X-Z plane and far-field parameters	17
3.1	Normalized far field radiation pattern for 2D two-slot antenna with air-substrate and source excitation at position 1 which is the centre (Figure 2.1 (b)) . . . . .	19
3.2	Normalized far field radiation pattern for 2D two-slot antenna with metamaterial substrate and source excitation at position 1 which is the centre (Figure 2.1 (b))	20
3.3	Normalized far field radiation pattern for 2D two-slot antenna with metamaterial substrate and source excitation at position 2 (Figure 2.1 (b)) . . . . .	20
3.4	Normalized far field radiation pattern v/s Azimuth angle plot comparing metamaterial substrate two-slot antenna with the air substrate medium, for: $f_p=f_o=1\text{GHz}$ , $SL=2\lambda_p$ , $h=\lambda_p$ , $SW=0.125\lambda_p$ and Spacing= $0.5\lambda_p$ . . . . .	21
3.5	Normalized far field radiation pattern v/s Azimuth angle plot comparing metamaterial substrate two-slot antenna with the air substrate medium, for: $SL=2\lambda_p$ , $h=\lambda_p$ , $SW=0.125\lambda_p$ and Spacing= $0.5\lambda_p$ . . . . .	22
3.6	Beam width pattern v/s Frequency plot comparing metamaterial substrate two-slot antenna with air substrate antenna, for: $f_p=f_o=1\text{GHz}$ , $SL=2\lambda_p$ , $h=\lambda_p$ , $SW=0.125\lambda_p$ and Spacing= $0.5\lambda_p$ . . . . .	22
3.7	Normalized far field pattern plot for a metamaterial slot antenna with different slot lengths, other constant values are: $f_p=1\text{GHz}$ , $SL=1\lambda_p, 2\lambda_p, 2.5\lambda_p, 3\lambda_p$ , $h=\lambda_p$ , $SW=0.125\lambda_p$ and Spacing= $0.5\lambda_p$ . . . . .	23

3.8	Beam width pattern plot for a metamaterial slot antenna with different slot lengths, other constant values are: $f_p=f_o=1\text{GHz}$ , $SL=1\lambda_p, 2\lambda_p, 2.5\lambda_p, 3\lambda_p$ , $h=\lambda_p$ , $SW=0.125\lambda_p$ and $\text{Spacing}=0.5\lambda_p$ . . . . .	24
3.9	Normalized far field pattern plot for MM with different slot widths $SW$ , other constant values are: $f_p f_o=1\text{GHz}$ , $SL=2\lambda_p$ , $h=\lambda_p$ , $\text{Spacing}=0.5\lambda_p$ and $SW=0.0625\lambda_p, 0.125\lambda_p$ and $0.25\lambda_p$ . . . . .	25
3.10	Beam width pattern plot for a metamaterial slot antenna with different slot widths, other constant values are: $f_p f_o=1\text{GHz}$ , $SL=2\lambda_p$ , $h=\lambda_p$ , $\text{Spacing}=0.5\lambda_p$ and $SW=0.0625\lambda_p, 0.125\lambda_p$ and $0.25\lambda_p$ . . . . .	25
3.11	Normalized far field pattern plot for a metamaterial slot antenna with different substrate thickness, other constant values are: $f_p=f_o=1\text{GHz}$ , $SL=2\lambda_p$ , $SW=0.125\lambda_p$ , $h=0.5\lambda_p, 1\lambda_p, 1.5\lambda_p$ and $\text{Spacing}=0.5\lambda_p$ . . . . .	26
3.12	Beam width pattern plot for a metamaterial slot antenna with different substrate thickness, other constant values are: $f_p=f_o=1\text{GHz}$ , $SL=2\lambda_p$ , $SW=0.125\lambda_p$ , $h=0.5\lambda_p, 1\lambda_p, 1.5\lambda_p$ and $\text{Spacing}=0.5\lambda_p$ . . . . .	27
3.13	Normalized far field pattern plot for a metamaterial slot antenna with different slot spacing, other constant values are: $f_p=f_o=1\text{GHz}$ , $SL=2\lambda_p$ , $SW=0.125\lambda_p$ , $h=1\lambda_p$ and $\text{Spacing}=0.25\lambda_p, 0.5\lambda_p$ and $1\lambda_p$ . . . . .	27
3.14	Beam width pattern plot for a metamaterial slot antenna with different slot spacing, other constant values are: $f_p=f_o=1\text{GHz}$ , $SL=2\lambda_p$ , $SW=0.125\lambda_p$ , $h=1\lambda_p$ and $\text{Spacing}=0.25\lambda_p, 0.5\lambda_p$ and $1\lambda_p$ . . . . .	28
3.15	Normalized far field pattern plot for free space and metamaterial substrate medium with different phi angle, other constant values are: $f_p=f_o=1\text{GHz}$ , $SL=2\lambda_p$ , $SW=0.125\lambda_p$ , $h=1\lambda_p$ and $\text{Spacing}=0.5\lambda_p$ . . . . .	29
3.16	Normalized far field pattern plot for different position of source shift towards the left along the X-axis for Freespace medium, other constant values are: $f_p=f_o=1\text{GHz}$ , $SL=2\lambda_p$ , $SW=0.125\lambda_p$ , $h=1\lambda_p$ and $\text{Spacing}=0.5\lambda_p$ . . . . .	29
3.17	Normalized far field pattern plot for different position of source shift towards the left along the X-axis for Metamaterial medium, other constant values are: $f_p=f_o=1\text{GHz}$ , $SL=2\lambda_p$ , $SW=0.125\lambda_p$ , $h=1\lambda_p$ and $\text{Spacing}=0.5\lambda_p$ . . . . .	30
3.18	Normalized far field pattern plot for different position of source shift towards the bottom along the Z-axis for Freespace medium, other constant values are: $f_p=f_o=1\text{GHz}$ , $SL=2\lambda_p$ , $SW=0.125\lambda_p$ , $h=1\lambda_p$ and $\text{Spacing}=0.5\lambda_p$ . . . . .	31
3.19	Normalized far field pattern plot for different position of source shift towards the bottom along the Z-axis for Metamaterial medium, other constant values are: $f_p=f_o=1\text{GHz}$ , $SL=2\lambda_p$ , $SW=0.125\lambda_p$ , $h=1\lambda_p$ and $\text{Spacing}=0.5\lambda_p$ . . . . .	31
4.1	(a) Side-view of multi-slot antenna array structure (b) Doppler Shift . . . . .	34

# List of Tables

3.1	Summary of our studies based on the various cases described . . . . .	32
-----	---	----

# Chapter 1

## Introduction

Metamaterials (MTMs) are broadly defined as “artificial effectively homogeneous electromagnetic structures with unusual properties not readily available in nature”. In [3] a special class of MTMs exhibit negative values of permittivity,  $\epsilon$  and permeability constant,  $\mu$ . Figure 1.1 shows materials with different combinations of permittivity and permeability and the nature of the resulting wave propagation within these mediums. The metamaterial based antennas as compared to conventional antennas show better performance in terms of directivity, gain, electric field strength etc. (as in Figure 1.4)

The researchers have proposed several structures (like periodic metallic structures) used to simulate materials with a dielectric or a magnetic plasma frequency based left-handed metamaterial. Under proper conditions of dispersive relative permittivity and relative permeability resulting in negative refractive index, cause a propagating plane wave in this media to form a left-handed triad (Electric field E, Magnetic field H and propagation constant k form a left-handed system). The other such types of metamaterials are double negative metamaterials (DNG), Epsilon negative media (ENG) like electronic plasmas, Mu negative media (MNG) like ferrimagnetic materials or gyromagnetic materials, near zero refractive index materials (NZIM) with directivity enhancement which we are focusing on in this thesis work. In these recent years the metamaterials are attracting a great deal of research and the reason being the fact that these structures (periodic metallic) provides means to control the propagation of electromagnetic waves. Under proper conditions (Figure 1.4 (c)), the energy radiated by source which is embedded in a slab

of metamaterial will be concentrated in a narrow cone in the surrounding media [8].

The directivity of an antenna can be increased either by increasing the aperture size or with large synthetic aperture using an array of antennas. These novel antenna types based on metamaterials are used in the applications such as portable interaction with satellite communications, Wi-Fi router, surveillance sensors, communication links, wireless broadcasting, navigation systems, convergent micro lenses and biomedical sensing applications such as heat applicator with beam scanning for interstitial microwave hyperthermia.

## 1.1 Organization of Thesis

The various sections of the thesis report are organized as follows:

Chapter 1 deals with the introduction of metamaterials, followed by describing the motivation for two-slot antenna design with double near zero metamaterial substrate for achieving high directivity. Then a brief history of various works in antenna applications based on metamaterial substrate for high directivity antenna design is presented.

Chapter 2 includes the problem statement which is described in detail with the proposed mathematical modelling of the problem.

Chapter 3 highlights the various important results and inferences obtained from the FDTD simulations.

Chapter 4 discusses about the conclusion and future work.

## 1.2 Metamaterial concepts

In 1967 Russian physicist Victor G. Veselago [18] considered the existence of a “substance with simultaneously negative values of  $\epsilon$  and  $\mu$ ” depicted in the III quadrant in Figure 1.1 and named these materials as left handed (LH) metamaterials since these materials allow the propagation of electromagnetic waves with the electric field, magnetic field and the phase constant vector satisfying a left-handed triad, compared with conventional materials where this triad is right handed i.e. the direction of propagation is opposite to that of direction of propagation in conventional type of materials. While various types of metamaterials like Left-handed (LH) metamaterial, Ep-

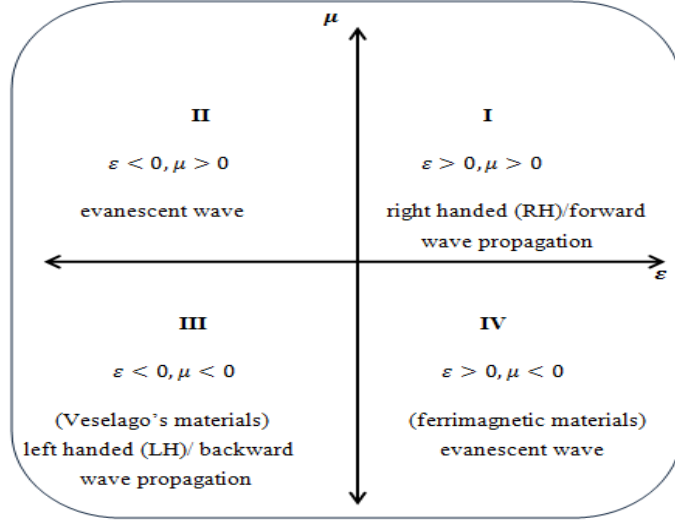


**Figure 1.1: Different combinations of  $\epsilon$  and  $\mu$  and type of wave propagation in that medium**

silicon Near Zero (ENZ), Mui Near Zero (MNZ), Double Negative medium (DNG) and Composite LH/RH metamaterial have been described in literature, in this thesis we will use metamaterials defined by the dispersive relative permittivity and permeability in equations shown below and having near zero refractive index (NZI) property.

$$\epsilon = \epsilon_o \left( 1 - \frac{\omega_p^2}{\omega^2} \right) \quad (1.1)$$

$$\mu = \mu_o \left( 1 - \frac{\omega_p^2}{\omega^2} \right) \quad (1.2)$$

where,  $\omega$  is frequency of source/excitation and  $\omega_p$  is plasma frequency of the metamaterial. The equations show Lorentz/Drude model for dispersive permittivity and permeability. Figure 1.1 shows the various quadrants of different values or ranges of permittivity and permeability, which form different material behaviour and property, giving rise to different wave propagation characteristics.

### 1.3 History of metamaterials for design of directive antennas

This section presents a brief history of different investigations which had been done for improving the antenna characteristics using metamaterial medium or metamaterial substrate.

In 2001, Ziolkowski [22] described the phenomena of wave propagation in the medium having

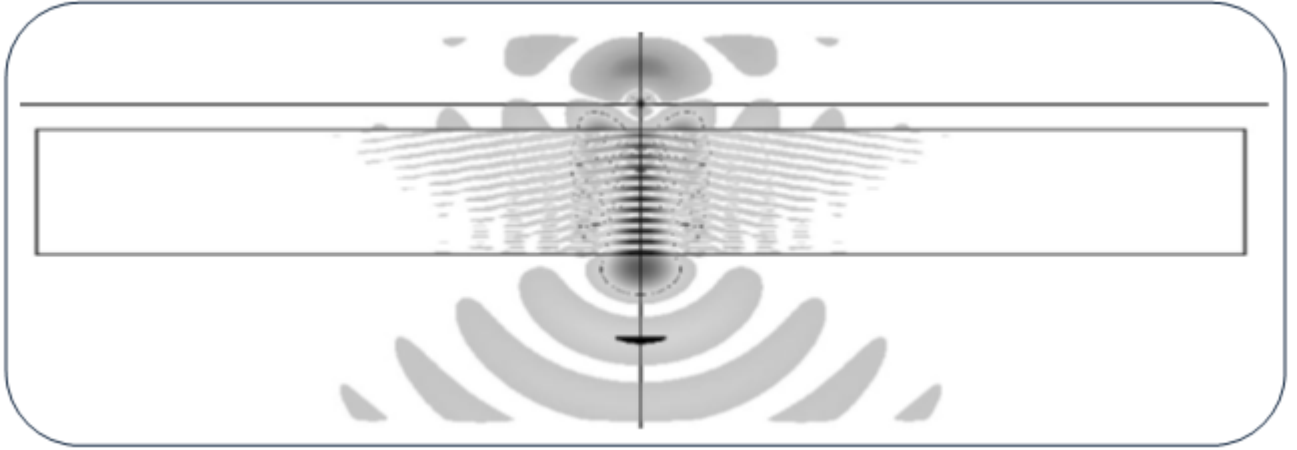
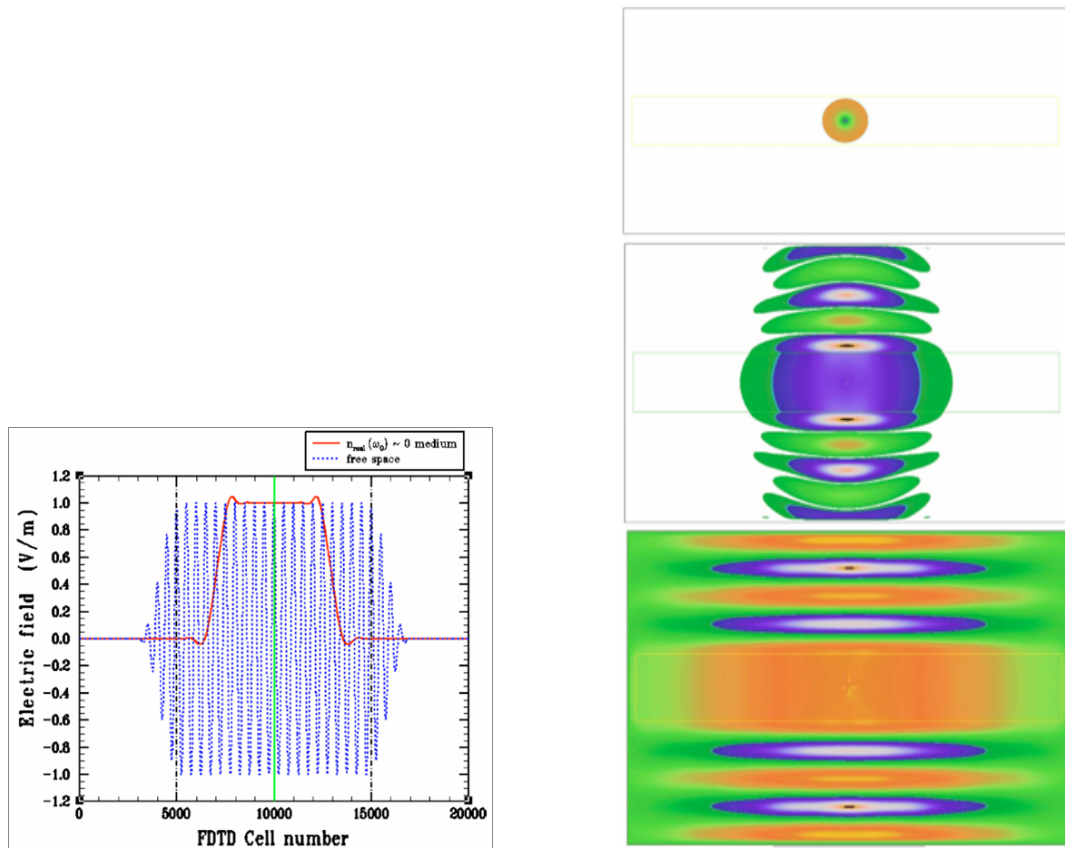


**Figure 1.2: 2-D FDTD simulation of wave propagation in metamaterial [3]. The source is kept outside the metamaterial medium.**

negative permittivity and negative permeability using finite difference time domain (FDTD) simulations. He explained that a perfect lens can be realized only for those frequencies where  $\epsilon(\omega)=\mu(\omega)=-1$ . Therefore perfect lens behaviour is only shown for  $\omega=\omega_p/\sqrt{2}$  in (1.1). In Figure 1.2, the results of a two-dimensional (2-D) FDTD simulation are shown. The metamaterial region with a plasma frequency of 80GHz is defined within rectangular box and the source is kept along the line just outside metamaterial region. This figure shows that the direction of the wave propagation changes inside the metamaterial when compared to free space outside the metamaterial.

Ziolkowski in 2004, in his paper "Propagation in and scattering from a matched metamaterial having a zero index of refraction", [21], simulated 1D and 2D FDTD structure and he concluded from the simulation results that within the matched zero-index substrate medium slab we obtain uniform electric field distribution showing the highly directional emissions as shown in Figure 1.3 (a). In the second Figure 1.3 (b) the source is located at the origin and one can see that the field radiated from zero-index substrate slab propagates away normal to the surface of slab. We can observe the uniform electric field distribution across the slab radiating coherently into the free space medium and within the slab we can observe the curved wavefronts being transformed into the planar wavefronts.

In 2002, Enoch [8] experimentally demonstrated that the unique characteristics of metamaterial defined by (1.1) and (1.2) can modify the emission of wave from an embedded source as shown in



(a) Electric field generated by an infinite current sheet driven by a 30 GHz source in a matched zero-index Drude medium slab and in free-space (b) Electric field distribution produced by a line source

Figure 1.3: Comparison of the electric field generated by an infinite current sheet driven by a 30 GHz source in a matched zero-index Drude medium slab and in free-space

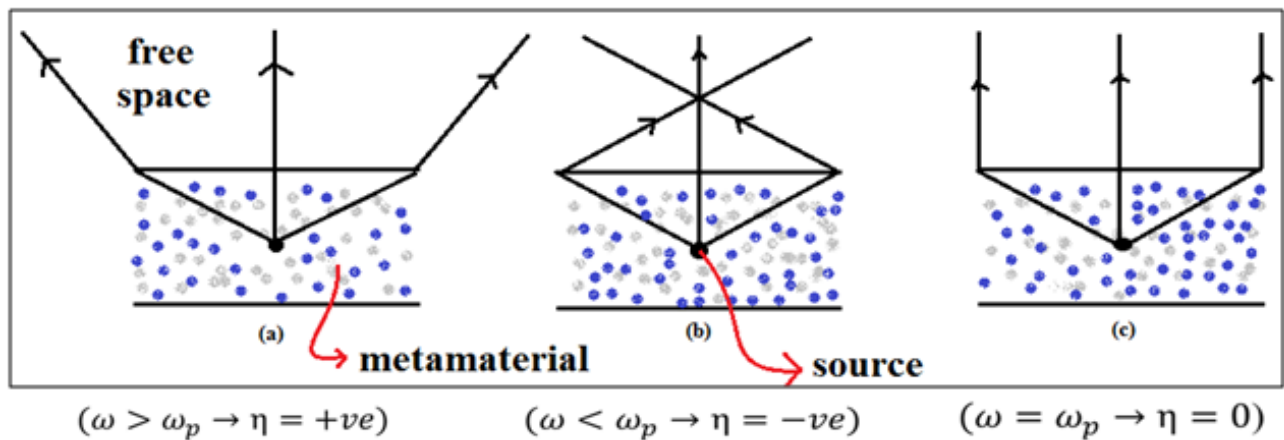


Figure 1.4: Different refraction scenarios when rays travel from metamaterial to free space medium.

Figure 1.4. He explained the two features of interest regarding the control of emission: direction and power of emission. The shaded region represents substrate material while the un-shaded region represents free space. As per Snell-Descartes law, incident waves from a point source embedded in a near-zero refractive index material will be refracted close to normal direction in a homogeneous right hand medium [8]. Note that the refractive index of the material is close to zero i.e. both  $\mu$  and  $\epsilon$  are zero when  $\omega=\omega_p$ , as angle of refraction would be close to zero. Using Snell's law of refraction ( $\sin\theta_t/\sin\theta_i=\mu_i/\mu_t$  where i denotes the incident medium and t denotes the transmitted medium,  $\theta$  is the angle and  $\mu$  is the refractive index), he showed that the rays are refracted in a direction close to normal, when  $\omega=\omega_p$  (Figure 1.4), if we consider the Lorentz/Drude model with homogeneous plasma-like dispersive permeability ( $\mu$ ) and permittivity ( $\epsilon$ ) as shown in (1.1) and (1.2) and refractive-index,

$$\eta = \pm\sqrt{\mu\epsilon} \quad (1.3)$$

In the other two cases, when  $\omega < \omega_p$  and  $\omega > \omega_p$  the rays either bend inwards or outwards respectively thereby decreasing the strength normal to interface. Therefore enhanced directivity can be realized when the refractive index of the material is near zero for a specific range of frequencies i.e., near the plasma frequency.

Further experimental verification of Enoch's results was carried out by Zhou [20] in year 2010, in which he embedded a monopole within a 2D metallic linear wire array. The wire array was designed such that the effective refractive index of the medium constituted by the array was close to zero at some specified frequency. The results showed improved directivity of the monopole for that specific frequency.

P. Baccarelli, P. Burghignoli, F. Frezza, A. Galli, P. Lampariello, G. Lovat, and S. Paulotto [1] in 2005, investigated the dispersive propagation and radiation properties of leaky waves on metamaterial grounded slabs. The proper or improper nature of the leaky modes supported by the metamaterial grounded slab depends on its double negative (DNG), permeability negative (MNG) or permittivity negative (ENG) characteristics of the dispersive medium which changes

with frequency. The associated frequency scan of the radiated beam through the broadside (conical radiation pattern) is illustrated by considering the field excited by dipole source placed in the infinite metamaterial grounded slab. G. Lovat, P. Burghignoli, F. Capolino, D. R. Jackson, and D. R. Wilton in 2006 [13] presented the analysis of directive radiation from a line source in a metamaterial slab with low permittivity.

Zi bin Weng in 2006 [19], proposed a new method to effectively improve the gain of patch antenna with metamaterial cover composed of ring aperture lattice. At 2.55 GHz, the gain of the metamaterial patch antenna was found to be 2.5 times greater than the gain of a conventional patch antenna and reduction in half power beam width was achieved due to the focusing of radiation energy.

The design of directive antennas that radiates away from the broadside direction is in demand in many of the emerging applications such as THz communication, biomedical, MEMS, implantable systems and energy harvesting, where on-chip antennas show immense potential in shaping up the future communication systems. H. M. Cheema and A. Shamim in 2013 [5] have presented a comprehensive overview of on-chip antennas that require high directivity, high gain, and beam steering characteristics. In view to this, near-zero refractive index substrates with slot antenna array could be identified as the means towards mitigation of the losses due to surface wave propagation through the silicon substrate and enhancing the directivity, gain and efficiency of the on-chip antenna in the desired direction.

The properties of near-zero refractive index metamaterials (ZIM) based different superstrates (ENZ-Epsilon  $\epsilon$  Near Zero, MNZ-Mui  $\mu$  Near Zero, DNZ- Double Near Zero) which can control the directive emission of a source have been researched by Haixia Liu, Yingchun Fan, Kai Zhou, Long Li, and Xiaowei Shi in 2014 [5]. They show experimentally that double near-zero (permittivity and permeability both are near zero, DNZ) metamaterial superstrate can converge the aperture E-field (Electric field) and H-field (Magnetic field) of the patch antenna (integrated with DNZ metamaterial) simultaneously. The maximum radiation directivity enhancement of 9.2dB can be obtained (15.7dBi).

Dongki Kim, Namgon Kim, Changyul Cheon, and Youngwoo Kwon in 2010 [10] developed planar covered multi-slot array heat applicator with beam scanning capability for the interstitial microwave hyperthermia, considering the biomedical applications. In this, they proposed an interstitial applicator based on multi-slot array structure, and by gradually varying the slot sizes it allows beam scanning capability according to the input frequencies. The choice of frequencies helps in generating concentrated beam at the designed slot positions, which provides focused heating and additional dimension of beam control. Another feature of this applicator is the low permittivity dielectric cover placed on top of the slot arrays to act as a protective layer against the heterogeneous biological material and a dielectric lens which assists to flatten the wave front to allow microwave radiation deeper into the heating material.

## 1.4 Problem Statement and Objectives

In this thesis we propose to investigate the use of a near zero refractive index based metamaterial substrate for building 3D slot antenna with high directivity at the broadside direction. Slot antennas are very popular because of their low profiles, ease of fabrication and frequency scanning capabilities. We demonstrate a directive 3D two-slot antenna structure with a near zero refractive index (NZI) substrate that is capable of directing the main lobe of the radiation pattern away from the broadside direction.

The main lobe shift is a function of the position of the source excitation within the substrate, with respect to the two slot apertures. We have used computational electromagnetic (EM) techniques for studying the wave propagation mechanisms in the simulated 3D antenna structure. Previously, Correa and Jin [6] in 2003 came up with theoretical analysis of left handed metamaterials using FDTD-PML (Finite Difference Time Domain-Perfectly Matched Layer) method. We use a similar analysis in this work.

In our case, we consider a broadband source (Gaussian pulse source) embedded inside a three dimensional (3D) waveguide with two slots and a DNZ substrate. The simulation space is enclosed by a perfectly matched layer. The time-domain electric field is obtained at every point in the two apertures using the Fourier transform and is simulated with FDTD simulations. The Z-transform technique which was originally proposed by Sullivan [15], are used for modeling the dispersive nature of permittivity and permeability of the substrate. The far field radiation pattern of the two-slot antenna is studied using field equivalence principles.

## Chapter 2

# Simulation Modeling

In this chapter of thesis work, we investigate the directivity and beam steering capability of a three-dimensional two-slot antenna with a metamaterial substrate. The problem space is modeled as a  $3\text{m} \times 2.7\text{m} \times 2.4\text{m}$  problem space in the XYZ Cartesian coordinate system space as shown in Figure 2.2 and the 3D simulation structure is shown in Figure 2.1. A waveguide of thickness  $h$ , with perfect electric conductor (PEC) walls and two rectangular slots in the XZ plane. The longer dimension of the slots are along the Z axis and they are separated by a distance of  $\lambda/2$  along the X axis. The region inside the waveguide is a metamaterial substrate with dispersive permeability and permittivity as shown below,

$$\epsilon = \epsilon_o \left( 1 - \frac{\omega_p^2}{\omega^2} \right) \quad \mu = \mu_o \left( 1 - \frac{\omega_p^2}{\omega^2} \right) \quad (2.1)$$

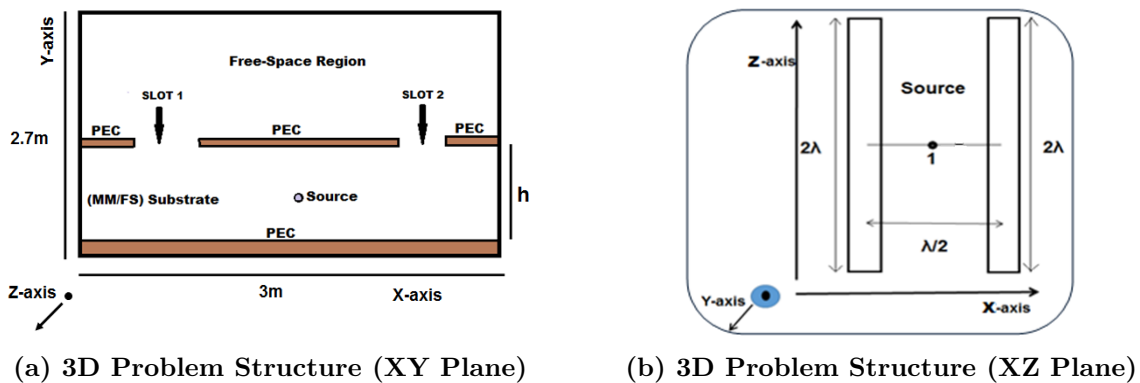


Figure 2.1: 3D Problem Structure top-view and side-view

where  $\omega$  is the source frequency and  $\omega_p$  is the plasma frequency of the metamaterial. The region outside the waveguide is free space with  $\epsilon=\epsilon_o$  and  $\mu=\mu_o$ . Two slot apertures of length  $SL=2\lambda$  are introduced in the waveguide placed along the x-axis and oriented along the z-axis.

The problem is modeled using 3D finite difference time domain (FDTD) technique in C code using Codeblock and simulations are done using MATLAB 2013b.

The antennas are excited by a TM mode Gaussian pulse source with a sigma spread of 0.208 ns.

## 2.1 Derivation of three dimensional (3D) FDTD equations

Three-dimensional FDTD simulation is much like two-dimensional simulations and for the derivation of 3D-FDTD equations for wave propagation with dispersive/frequency dependent permittivity and permeability values, we revisit the two of Maxwell's equations for electric and magnetic fields as shown in (2.2) and (2.3).

$$\textit{Faraday'sLaw} : \quad \nabla \times \vec{E} = -\frac{\partial \vec{B}}{\partial t} \quad (2.2)$$

$$\textit{Ampere'sCircuitalLaw} : \quad \nabla \times \vec{H} = \sigma \vec{E} + \frac{\partial \vec{D}}{\partial t} \quad (2.3)$$

where  $\vec{E}$  is electric field intensity,  $\vec{H}$  is magnetic field intensity,  $\vec{B}$  is magnetic flux density and  $\vec{D}$  is electric flux density and we consider TM (Transverse Magnetic) mode of propagation.

The other two Maxwell's equations are automatically satisfied due to the divergence-free nature of the FDTD Yee cell shown in Figure 2.2 taken from [11].

We use equations (2.1) for calculating  $\epsilon$  and  $\mu$  and for modeling the PEC (Perfect Electric Conductor) walls, permittivity  $\epsilon$  is modified in order to include the effect of frequency since permittivity and permeability is dispersive for metamaterials. The Lorentz/Drude model in frequency domain for dispersive materials can be expressed as:

$$\textit{Since, } D_z(\omega) = \epsilon_r(\omega).E_z(\omega), \textit{ Drude/LorentzModel} : \epsilon_r(\omega) = \epsilon_\infty - \left( \frac{\omega_p^2}{\omega^2 + j\omega\gamma} \right) \quad (2.4)$$

where  $\epsilon_r(\omega)$  is the dispersive relative permittivity,  $\epsilon_\infty$  is the relative permittivity in the infinity

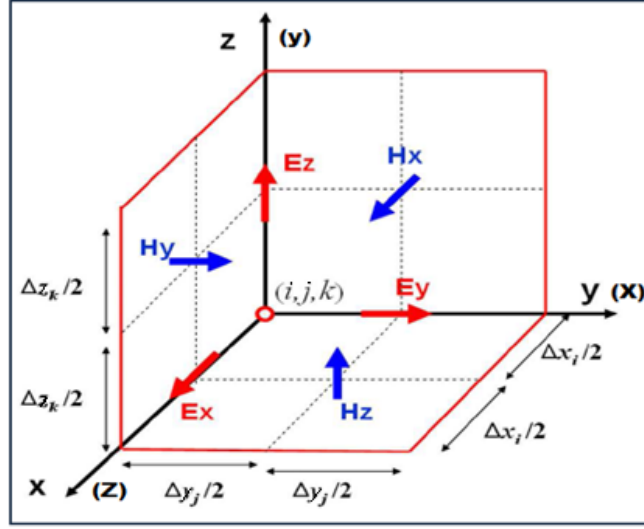


**Figure 2.2:** Structure of the Yee cell located at  $(i,j,k)$ . 6 field components  $(E_x, E_y, E_z, H_x, H_y, H_z)$  are arranged around  $(i,j,k)$  with half grid differences satisfying the Maxwell's equations.  $(x), (y), (z)$  is the axis considered for problem formulation.

frequency,  $D_z$  and  $E_z$  are components of  $\vec{D}$  and  $\vec{E}$  in the z-direction,  $\omega_p$  is plasma frequency of the metamaterial substrate,  $\omega$  is operating frequency and  $\gamma$  is the damping factor or collision frequency.

Maxwell's Ampere Circuital law curl equation can be expressed as,

$$\frac{\partial H_z}{\partial t} = \frac{1}{\mu} \left[ \frac{\partial E_x}{\partial y} - \frac{\partial E_y}{\partial x} \right] \quad (2.5)$$

where  $H_z$  is z-component of magnetic field H,  $E_x$  &  $E_y$  is x and y component of electric field E.

Using the Yee's algorithm or leapfrog method of central differences approximation,

$$\frac{H_z \Big|_{(i+\frac{1}{2}, j+\frac{1}{2}, k)}^{n+1/2} - H_z \Big|_{(i+\frac{1}{2}, j+\frac{1}{2}, k)}^{n-1/2}}{\Delta t} = \frac{1}{\mu \Big|_{(i+\frac{1}{2}, j+\frac{1}{2}, k)}} \left[ \frac{\left( E_x \Big|_{(i+\frac{1}{2}, j+1, k)}^n - E_x \Big|_{(i+\frac{1}{2}, j, k)}^n \right)}{\Delta y[j]} - \frac{\left( E_y \Big|_{(i+1, j+\frac{1}{2}, k)}^n - E_y \Big|_{(i, j+\frac{1}{2}, k)}^n \right)}{\Delta x[i]} \right] \quad (2.6)$$

Expressing these in terms of memory position (discrete) and where i, j and k represent discrete

space along the x, y and z-axis respectively, and n represents the discrete time.

$$H_z[i][j][k] = H_z[i][j][k] + \frac{\Delta t}{\mu[i][j][k]} \left[ \frac{1}{\Delta y[j]} \left( E_x[i][j+1][k] - E_x[i][j][k] \right) - \frac{1}{\Delta x[i]} \left( E_y[i+1][j][k] - E_y[i][j][k] \right) \right] \quad (2.7)$$

Similarly, the FDTD update equation for the Ez component of electric field is,

$$\frac{E_z \Big|_{(i,j,k+\frac{1}{2})}^{n+1/2} - E_z \Big|_{(i,j,k+\frac{1}{2})}^n}{\Delta t} = \frac{1}{\epsilon \Big|_{(i,j,k+\frac{1}{2})}} \left[ \frac{\left( H_x \Big|_{(i,j+\frac{1}{2},k+\frac{1}{2})}^{n+\frac{1}{2}} - H_x \Big|_{(i,j-\frac{1}{2},k+\frac{1}{2})}^{n+\frac{1}{2}} \right)}{\Delta y[j]} - \frac{\left( H_y \Big|_{(i+\frac{1}{2},j,k+\frac{1}{2})}^{n+\frac{1}{2}} - H_y \Big|_{(i-\frac{1}{2},j,k+\frac{1}{2})}^{n+\frac{1}{2}} \right)}{\Delta x[i]} \right] \quad (2.8)$$

Further simplifying these equations and then expressing in terms of memory gets us to the discrete time domain equations,

$$E_z[i][j][k] = E_z[i][j][k] + \frac{\Delta t}{\epsilon[i][j][k]} \left[ \frac{1}{\Delta y[j]} \left( H_x[i][j][k] - H_x[i][j-1][k] \right) + \frac{1}{\Delta x[i]} \left( H_y[i][j][k] - H_y[i-1][j][k] \right) \right] \quad (2.9)$$

FDTD is a direct space-time approach and the basic algorithm of FDTD method depends on Maxwell's equations. We can note from these equations that there exists  $\frac{1}{2}$  time difference in the update equations for the E-field and H-field data, so sequential updates of the E-field and H-field complete one FDTD time stepping. At a particular time point (n), E-field data are updated and stored in memory using H-field data previously  $\left( n - \frac{1}{2} \right)$  stored in the memory. Then at time of  $\left( n + \frac{1}{2} \right)$ , H-field data is updated and stored in the memory by using the E-field data which was computed in the previous case. This process continues and we get complete information on the electromagnetic fields in space and time.

In order to achieve the stability condition for 3D-FDTD method (Courant condition), the relation between the time variation and spatial variation is,

$$\Delta t \leq \frac{1}{c \left( \sqrt{\left( \frac{1}{(\Delta x)^2} + \frac{1}{(\Delta y)^2} + \frac{1}{(\Delta z)^2} \right)} \right)} \quad (2.10)$$

where,  $\Delta x$  is the minimum edge length (grid size) along the x-direction, similarly  $\Delta y$  along y-direction and  $\Delta z$  is along the z-direction.

$$\Delta t = \frac{1}{cS} \quad (2.11)$$

where,  $c$ =speed of light and  $S$ =Courant Stability Factor

## 2.2 Derivation of far field equations of an aperture antenna from near field equations

We explain the basic concept of efficient far-field computation. FDTD simulations enable us to formulate and calculate the time domain near field values within the problem space and using the Fourier transform we calculate the frequency domain near field values. To calculate the normalized far field at the apertures and directivity, analysis must be done in the far field as per geometry shown in Figure 2.3. To obtain the far-field radiation pattern, we consider the radiation vectors that are sufficiently far ( $r \gg \lambda$ ) from the emitter source since all the field components (E and H) are assumed to fall off as  $1/r$ , typical of radiation fields. The direct application of the FDTD method would be difficult in terms of limited computer memory size and computation time and speed, and so we can efficiently obtain the far-field radiation by combining the 3D FDTD method and near-to-far field transformation formulae.

According to the field surface equivalence theorem introduced in 1936 by Schelkunoff [14] and based on the uniqueness theorem states [9] that “a field in a lossy region is uniquely specified by the sources within the region plus the tangential components of the electric field over the boundary, or the tangential components of the magnetic field over the boundary, or the former over part of the boundary and the latter over the rest of the boundary”. This theorem is applicable for lossless medium as well. Hence, if the tangential components of electric and magnetic fields are completely known over a closed surface  $\Omega$ , then we can determine the fields in the source-free region. The surface equivalence theorem can be explained in the Figure 2.4 where we assume that there exists  $\mathbf{E}$  and  $\mathbf{H}$  fields inside the surface  $\mathbf{S}$  and fields  $\mathbf{E}_1$  and  $\mathbf{H}_1$  outside the surface  $\mathbf{S}$  and for these fields to exist within and outside  $\mathbf{S}$ , they must satisfy

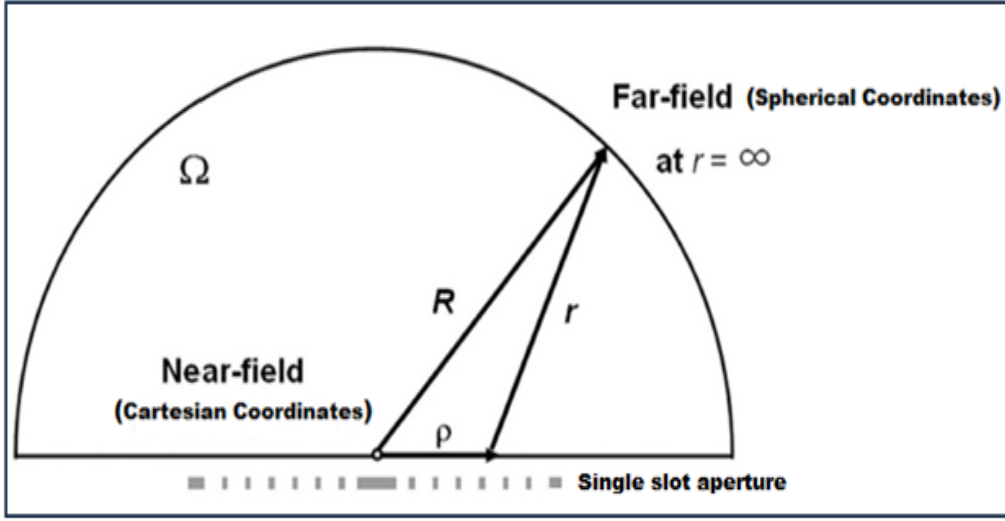


Figure 2.3: Geometry used for the far-field computation [11]

the boundary conditions about the tangential components of electric and magnetic field. The equivalent electric current density ( $\vec{J}_s$ ) and magnetic current density ( $\vec{M}_s$ ) on the surrounding surface can substitute all the information on the fields out of the space  $\Omega$  satisfying the boundary conditions such that  $\vec{J}_s$  and  $\vec{M}_s$  are calculated by the formulae below.

$$\vec{M}_s = -2(\vec{E}_a \times \hat{n}) \quad \text{and} \quad \vec{J}_s = 2(\vec{H}_a \times \hat{n}) \quad (2.12)$$

where,  $\hat{n}$  is the unit normal vector on the surface, and  $(\vec{J}_s)$  and  $(\vec{M}_s)$  are electric and magnetic current source across the aperture.

The tangential component of electric field along the perfect electric conductor (PEC) is zero but non-zero in the two slot apertures and this implies that boundary conditions along the slot interface can be modeled as a non-zero magnetic surface current density,  $\vec{M}_s$  along the aperture and  $\vec{J}_s = 0$ .

Using field equivalence principles,  $\vec{M}_s$  is given by (2.12) where  $\hat{n}$  is the unit vector perpendicular to the surface (aperture in X-Z plane),  $\vec{E}_a$  is the phasor electric field computed through Fourier transform of the time domain aperture field which is obtained by using FDTD method, hence

$$\vec{M}_s = -2(\vec{E}_a \times \hat{y}) \quad (2.13)$$

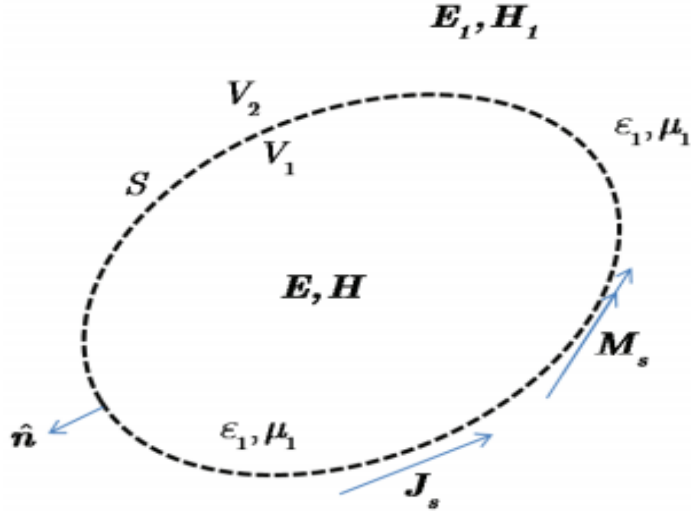


**Figure 2.4: Diagram to explain Surface Equivalence Theorem**

The electric vector potential,  $\vec{F}$  is related to  $\vec{M}_s$  through the equation,

$$\vec{F}(\vec{r}) = \frac{1}{4\pi} \int \left( \vec{M}_s(r') \frac{e^{-jk|\vec{r}-\vec{r}'|}}{|\vec{r}-\vec{r}'|} \right) \quad (2.14)$$

where  $|\vec{r}-\vec{r}'|$  is used to compute the far field component.

$$|\vec{r}-\vec{r}'| = \sqrt{(x-x')^2 + (y-y')^2 + (z-z')^2} \quad (2.15)$$

The primed parameters indicate the source (along the aperture: X-Z plane ( $x'$  and  $z'$ ) and at  $y'$ =centre) while the unprimed parameters ( $x, y, z$ ) are the scattered field or the far field (Figure 2.5)

The Electric field in the far field is obtained by:

$$\vec{E} = \vec{\nabla}_r \times \vec{F} \quad (2.16)$$

Combining equations (2.14), (2.15) and (2.16) we get the following:

$$\vec{E} = \frac{1}{4\pi} \left[ \vec{\nabla}_r \times \int (\vec{M}_s(r') \frac{e^{-jk|\vec{R}|}}{|\vec{R}|} dl \right] \quad (2.17)$$

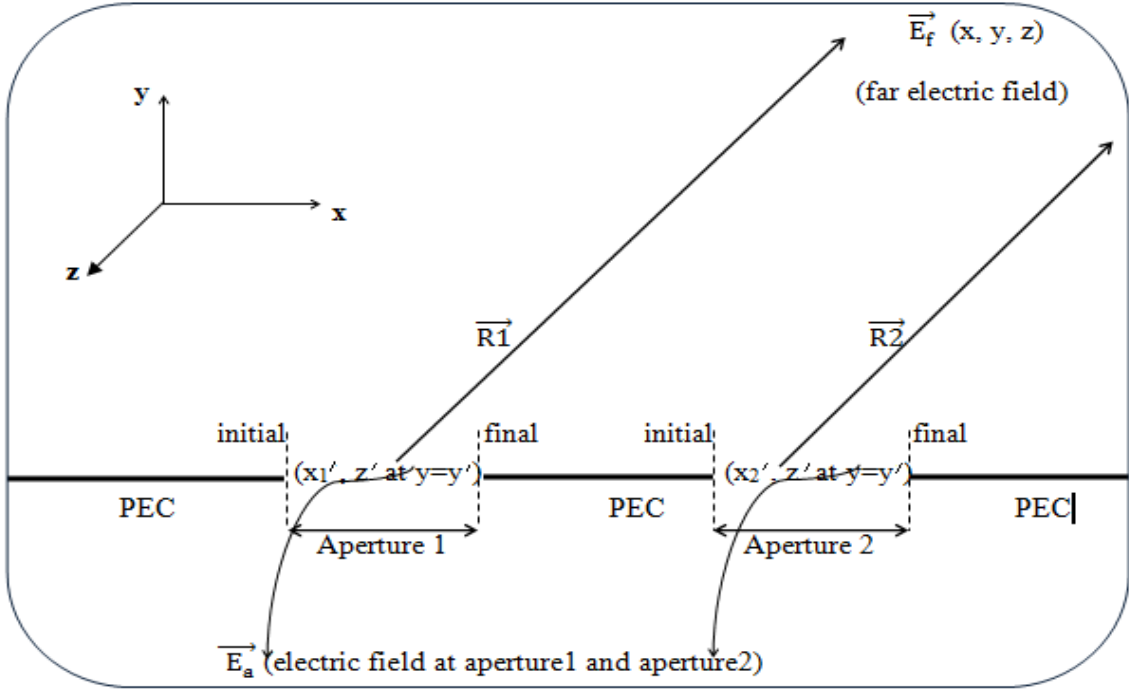


**Figure 2.5: Pictorial representation of aperture placed in X-Z plane and far-field parameters**

where  $|\vec{R}| = |\vec{r} - \vec{r}'|$  and  $dl$  is unit length in the aperture (here,  $dl$  is basically the unit length in the aperture for  $x$ -axis along which the slots are placed  $dx'$  and unit length for  $z$ -axis along which the slots are oriented  $dz'$ ).

Further simplifying leads to E field over the aperture  $dx' dz'$  as aperture is in X-Z plane:

$$\vec{E} = -\frac{1}{4\pi} \int \int \left[ (\vec{M}_s(r') \times \hat{r}) \left( jk + \frac{1}{|\vec{R}|} \right) \cdot \frac{e^{-jk|\vec{R}|}}{|\vec{R}|} \right] dx' dz' \quad (2.18)$$

The value of field at aperture is due to  $z$ -polarized plane wave (Gaussian source) and direction normal to the aperture in X-Z plane is  $y$  direction. We use  $jk = j\omega/c_0$  and ignore the  $1/R^2$  terms due to far field considerations. Therefore (2.18) reduces to the following:

$$\vec{E}_f(x, y, z, \omega) = \frac{1}{2\pi} \sum_{c=initial}^{final} \left[ r_y \vec{E}_{ac}(x', z', \omega) (jk) \cdot \frac{e^{-jk|\vec{R}|}}{|\vec{R}|} \right] \Delta l \quad (2.19)$$

where, (Figure 2.5) initial = initial aperture position co-ordinate, final = final aperture position co-ordinate,  $(\vec{E}_{ac})$  = Electric field at aperture position  $c$ ,  $\Delta l$  = length of one cell along  $x$ -axis and  $z$ -axis,  $r_y$  = component of  $\vec{R}$  in  $y$  direction

# Chapter 3

## Results

In this chapter of thesis work we have compared the performance of the proposed ‘3D two-slot antenna with metamaterial substrate’ with the performance of a ‘conventional slot antenna with an air substrate’ for different operating frequency  $f_o = f_p$ ,  $f_o < f_p$  and  $f_o > f_p$  and have investigated the beam steering behaviour of two-slot antenna. We have analyzed the effect of the following parameters on the antenna characteristics:

- (a) The plasma frequency,  $f_p$
- (b) The slot length (SL) in terms of wavelength  $\lambda$  corresponding to the plasma frequency
- (c) The slot width (SW) in terms of wavelength  $\lambda$
- (d) The thickness or height of the substrate (h) in terms of  $\lambda$
- (e) Distance or spacing between the slots
- (f) Variation in normalized far field for different azimuth angle  $\phi$  and elevation angle  $\theta$
- (g) Position of source along X-axis
- (h) Position of source along Z-axis

For each case, we study the radiation (normalized far field pattern v/s azimuth angle) characteristics of the antenna as a function of the parameters.

The results obtained from the two-dimensional (2D) two-slot structure design have been illustrated in the first part of the Chapter 3.

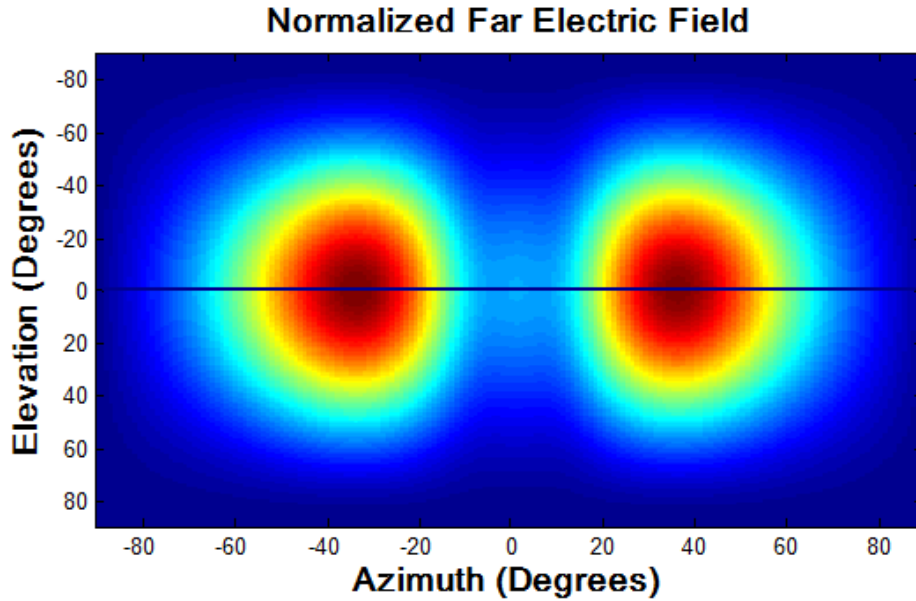


Figure 3.1: Normalized far field radiation pattern for 2D two-slot antenna with air-substrate and source excitation at position 1 which is the centre (Figure 2.1 (b))

### 3.1 Results for far-field radiation pattern for 2D two-slot antenna design:

The far-field radiation beam pattern of each slot in the 2D two-slot antenna design is governed by the combination of the array factor due to the two-slot antennas and their elemental pattern which is shown in Figure 3.1, 3.2 and 3.3, where the azimuth beam width is governed by the element pattern while the elevation beam width is governed by the array factor.

In Figure 3.1, the beam pattern of the 2D two-slot structure with the air-substrate medium is shown when the source excitation is place at the centre or position 1 (Figure 2.1 (b)).

In Figure 3.2, the beam pattern of the 2D two-slot structure with the metamaterial-substrate medium is shown when the source excitation is place at the centre or position 1 (Figure 2.1 (b)).

In Figure 3.3, the beam pattern of the 2D two-slot structure with the metamaterial-substrate medium is shown when the source excitation is place at the position 2 (shifted away from the centre) (Figure 2.1 (b)).

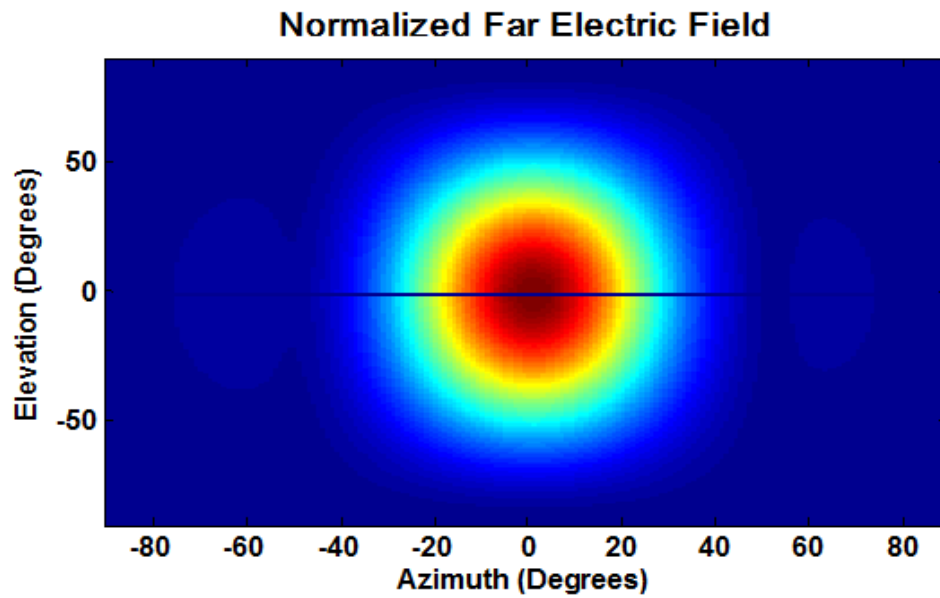


Figure 3.2: Normalized far field radiation pattern for 2D two-slot antenna with metamaterial substrate and source excitation at position 1 which is the centre (Figure 2.1 (b))

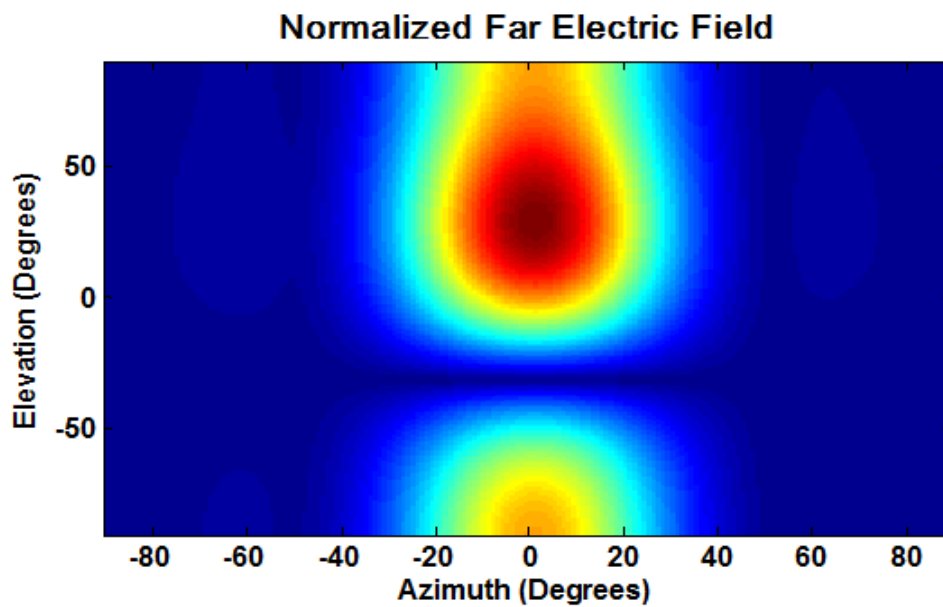
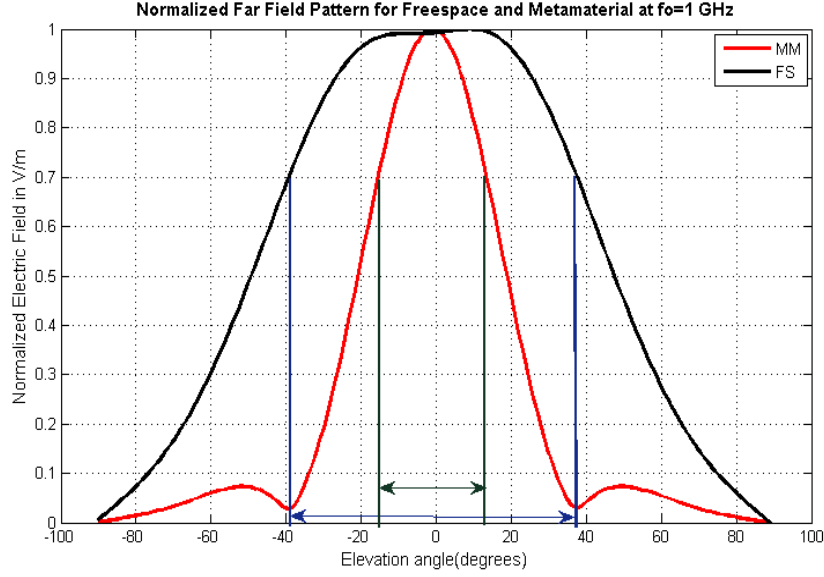


Figure 3.3: Normalized far field radiation pattern for 2D two-slot antenna with metamaterial substrate and source excitation at position 2 (Figure 2.1 (b))



**Figure 3.4:** Normalized far field radiation pattern v/s Azimuth angle plot comparing metamaterial substrate two-slot antenna with the air substrate medium, for:  $f_p=f_o=1\text{GHz}$ ,  $SL=2\lambda_p$ ,  $h=\lambda_p$ ,  $SW=0.125\lambda_p$  and  $\text{Spacing}=0.5\lambda_p$

## 3.2 Results for far-field radiation pattern for 3D two-slot antenna design:

### 3.2.1 Case (I)

The overall improvement due to a metamaterial substrate with  $f_p=1\text{ GHz}$ , thickness  $h=1\lambda_p=0.3\text{m}$ , and slot length,  $SL=2\lambda_p=0.6\text{m}$ , is compared with a similar dimension antenna structure with free-space or air substrate medium in Figure 3.4 and 3.6. Using the techniques described in the previous chapter, we compute the normalized far field radiation patterns. The far field pattern v/s azimuth angle plot in Figure 3.4 and beam width v/s frequency plot in Figure 3.6 was calculated for a radial distance of 100m along the azimuth plane. We observe that the directivity of the two-slot antenna with the metamaterial substrate is superior to the two-slot antenna with the air substrate medium. We note that there is a significant improvement in directivity for a bandwidth of frequencies around  $\omega = \omega_p$  ( $\omega_p = 2\pi f_p$ ) as compared to the conventional slot. The plot shows that the directivity is improved at the operating frequency equal to the plasma frequency  $f_o = f_p$  (1 GHz) as compared to the conditions when  $f_o < f_p$  (0.5 GHz) or  $f_o > f_p$  (1.7 GHz) as shown in Figure 3.5.

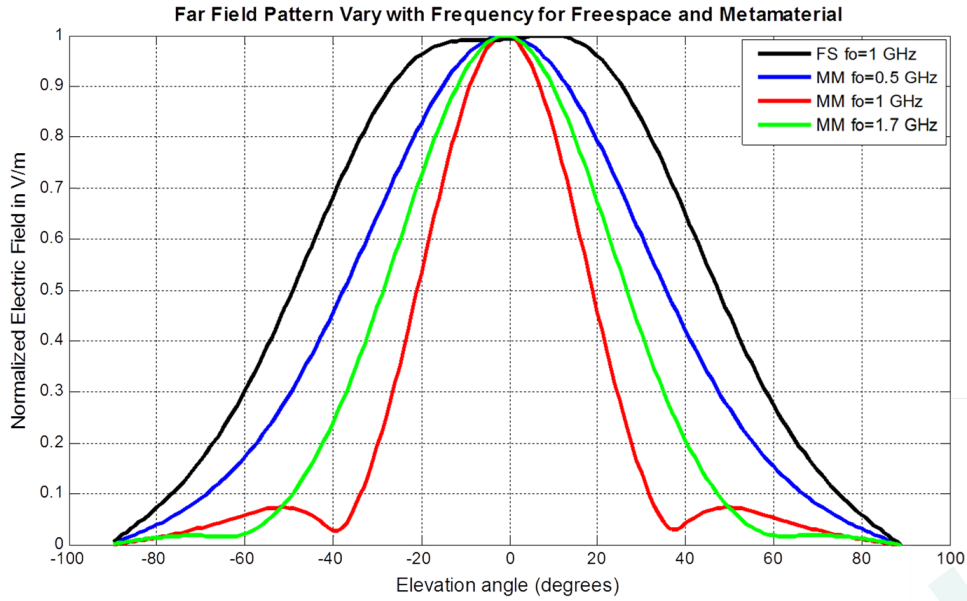


Figure 3.5: Normalized far field radiation pattern v/s Azimuth angle plot comparing metamaterial substrate two-slot antenna with the air substrate medium, for:  $SL=2\lambda_p$ ,  $h=\lambda_p$ ,  $SW=0.125\lambda_p$  and Spacing= $0.5\lambda_p$

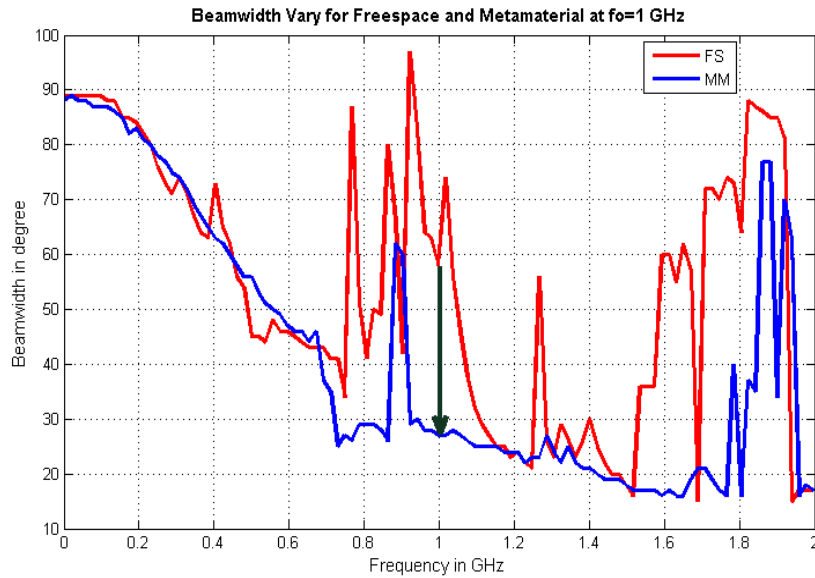
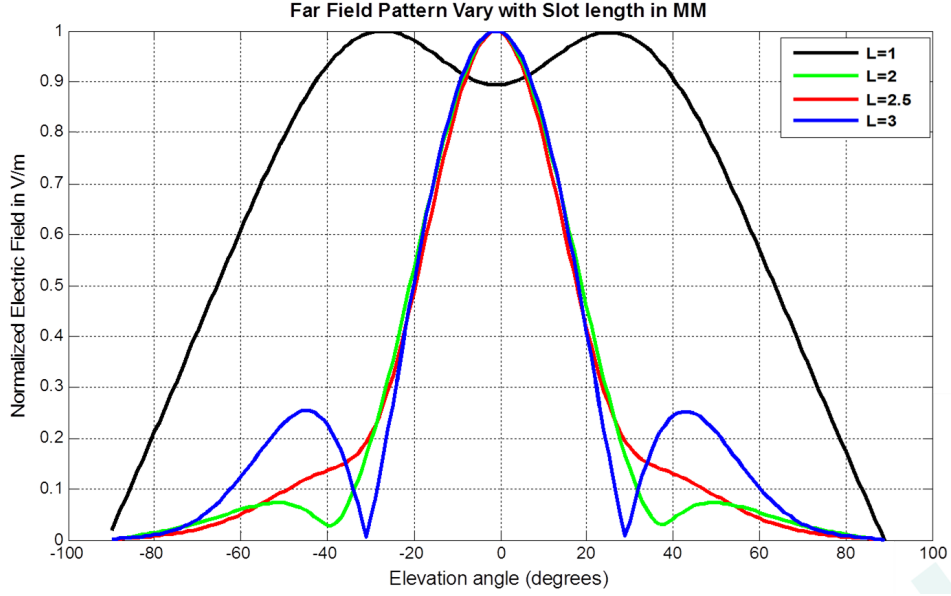


Figure 3.6: Beam width pattern v/s Frequency plot comparing metamaterial substrate two-slot antenna with air substrate antenna, for:  $f_p=f_o=1\text{GHz}$ ,  $SL=2\lambda_p$ ,  $h=\lambda_p$ ,  $SW=0.125\lambda_p$  and Spacing= $0.5\lambda_p$



**Figure 3.7:** Normalized far field pattern plot for a metamaterial slot antenna with different slot lengths, other constant values are:  $f_p=1\text{GHz}$ ,  $SL=1\lambda_p, 2\lambda_p, 2.5\lambda_p, 3\lambda_p$ ,  $h=\lambda_p, SW=0.125\lambda_p$  and  $\text{Spacing}=0.5\lambda_p$

### 3.2.2 Case (II)

In this case, we vary the length of the slot (along x-axis) while  $f_p$  is kept constant ( $f_o=f_p=1\text{GHz}$ ) and thickness of substrate  $h=1\lambda_p=0.3\text{m}$ . We observe that the directivity improves with increase in slot length in Figure 3.7 and 3.8 and for smaller slot length the metamaterial behavior is less dominant. The reduction in beam width is more when  $L$  is changed from 1 to 2 where  $L$  is the ratio of slot length and  $\lambda_p$ .

$$\text{Here,} \quad L = \frac{SL}{\lambda_p} \quad (3.1)$$

When we increase the slot length  $SL$  from  $2\lambda_p$  to  $3\lambda_p$ , the improvement in directivity is more and it shows an interesting tradeoff between the bandwidth and directivity.

### 3.2.3 Case (III)

In this case, we vary the width of the slot (along z-axis) while  $f_p$  is kept constant (1 GHz), slot length  $SL=2\lambda_p=0.6\text{m}$ , slot spacing= $0.5\lambda_p$  and thickness of substrate  $h=1\lambda_p=0.3\text{m}$ . We observe from the Figure 3.9 and 3.10 that the directivity remains constant with increase in slot width

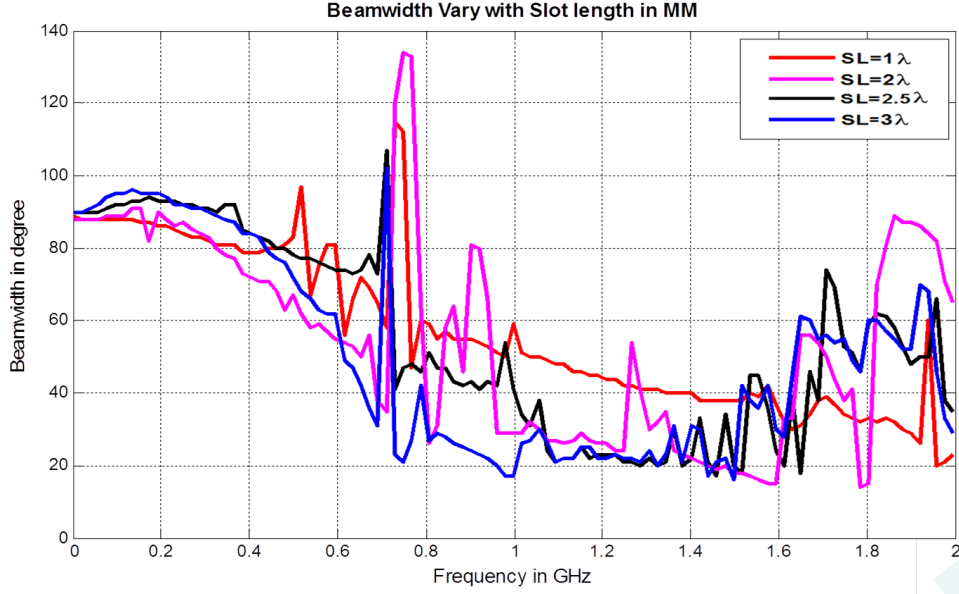


**Figure 3.8:** Beam width pattern plot for a metamaterial slot antenna with different slot lengths, other constant values are:  $f_p=f_o=1\text{GHz}$ ,  $SL=1\lambda_p$ ,  $2\lambda_p$ ,  $2.5\lambda_p$ ,  $3\lambda_p$ ,  $h=\lambda_p$ ,  $SW=0.125\lambda_p$  and  $\text{Spacing}=0.5\lambda_p$

in Figure 3.10 and 3.11. There is no variation in directivity when  $W$  is changed from 0.0625 to 0.25 where  $W$  is the ratio of slot width and  $\lambda_p$ .

$$\text{Here,} \quad W = \frac{SW}{\lambda_p} \quad (3.2)$$

### 3.2.4 Case (IV)

In this case, we analyze the effect of variation in thickness or height of substrate  $h$  while keeping other parameters constant:  $f_p=1\text{GHz}$ , width of the slots,  $SW=\lambda_p/8$  and length of the two slots,  $SL=2\lambda_p$ . This slot length and slot width is selected due to the reasons explained in Case II and Case III. From the far field pattern plot in Figure 3.11 and 3.12, we observe that there is not much improvement in directivity with increasing thickness of substrate from  $h=1\lambda_p$  to  $1.5\lambda_p$  but it seems to quickly converge as  $T$  increases. While when the thickness of the substrate  $h$  is increased from  $h=0.5\lambda_p$  to  $1\lambda_p$ , there is considerable improvement in the directivity of the far-field pattern.

$$\text{Here,} \quad T = \frac{h}{\lambda_p} \quad (3.3)$$

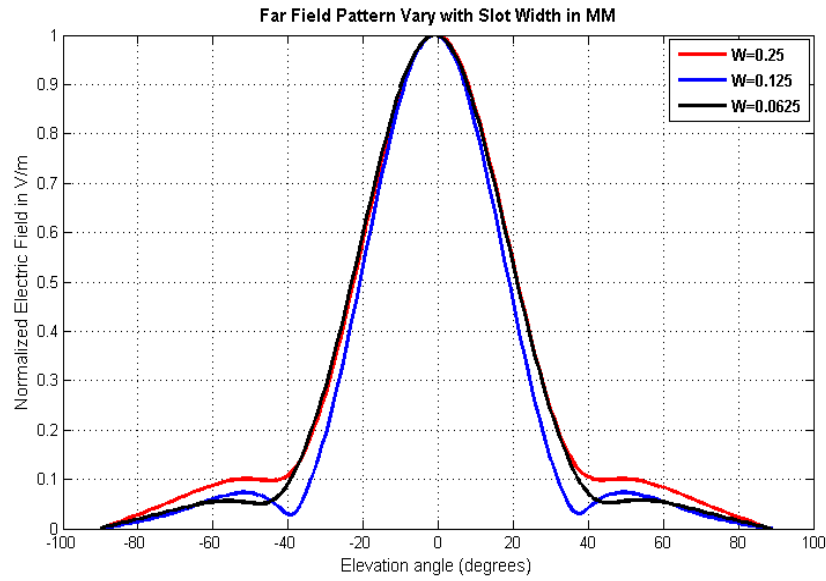


Figure 3.9: Normalized far field pattern plot for MM with different slot widths SW, other constant values are:  $f_p f_o=1\text{GHz}$ ,  $SL=2\lambda_p$ ,  $h=\lambda_p$ , Spacing= $0.5\lambda_p$  and  $SW=0.0625\lambda_p$ ,  $0.125\lambda_p$  and  $0.25\lambda_p$

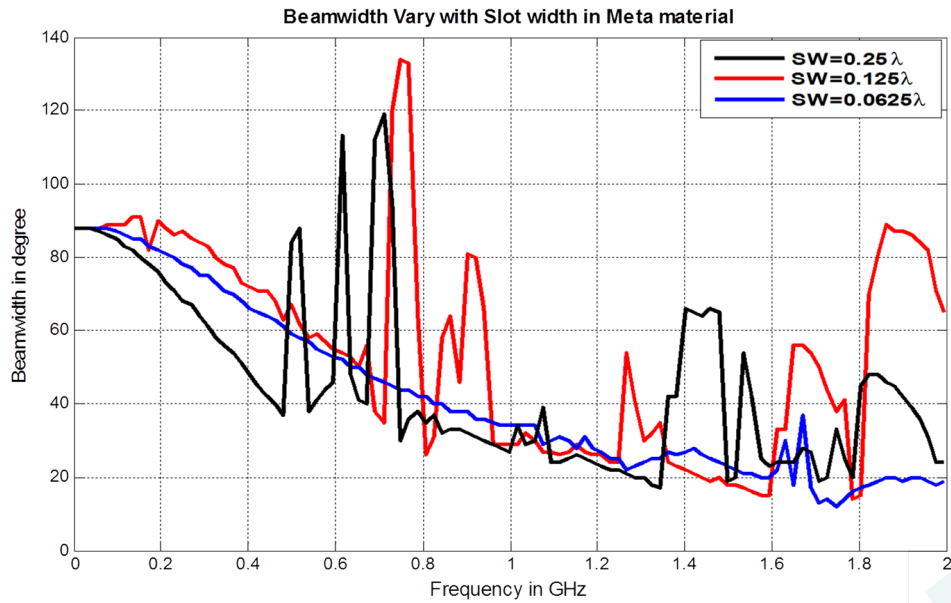
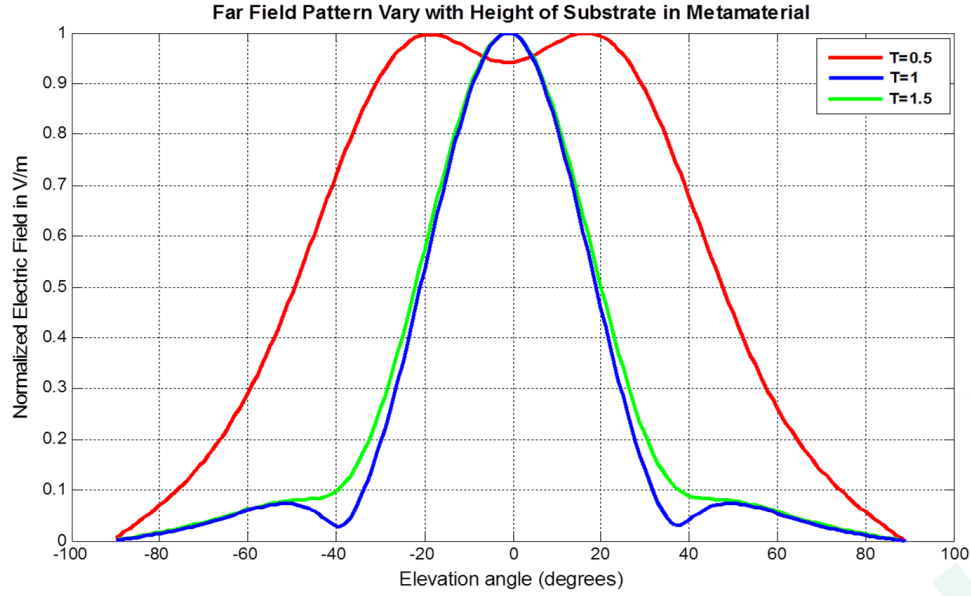


Figure 3.10: Beam width pattern plot for a metamaterial slot antenna with different slot widths, other constant values are:  $f_p f_o=1\text{GHz}$ ,  $SL=2\lambda_p$ ,  $h=\lambda_p$ , Spacing= $0.5\lambda_p$  and  $SW=0.0625\lambda_p$ ,  $0.125\lambda_p$  and  $0.25\lambda_p$



**Figure 3.11: Normalized far field pattern plot for a metamaterial slot antenna with different substrate thickness, other constant values are:  $f_p=f_o=1\text{GHz}$ ,  $SL=2\lambda_p$ ,  $SW=0.125\lambda_p$ ,  $h=0.5\lambda_p$ ,  $1\lambda_p$ ,  $1.5\lambda_p$  and Spacing= $0.5\lambda_p$**

### 3.2.5 Case (V)

In this case, we consider the variation of the normalized far field pattern or directivity and beam width of 3D two-slot antenna with distance or spacing between the two slots, while keeping the position of source at the centre of the two slots, while slot length, slot width and thickness of substrate constant:  $f_o=f_p=1\text{GHz}$ ,  $SL=2\lambda_p$ ,  $SW=0.125\lambda_p$  and  $h=1\lambda_p$ . It is observed in Figure 3.13 and 3.14 that the normalized far field pattern shows better directivity when spacing between the slots is changed from Spacing= $1\lambda_p$  to  $0.5\lambda_p$ , while there is not much improvement in directivity when spacing is changes from Spacing= $0.5\lambda_p$  to  $0.25\lambda_p$ . The array factor theory explains that when the spacing between the antenna array elements is within  $0.5\lambda_p$  then there are no grating lobes, while when the distance between the slots is increased beyond  $0.5\lambda_p$  then the grating lobes starts getting formed. These grating lobes being of the equal strength as that of the desired main lobe, it reduces the signal strength of the main lobe, decreasing its directivity.

### 3.2.6 Case (VI)

In this case, we consider the variation of the normalized far field pattern or directivity with the varying azimuth angle  $\phi$  for the free space and metamaterial substrate medium, while keeping the

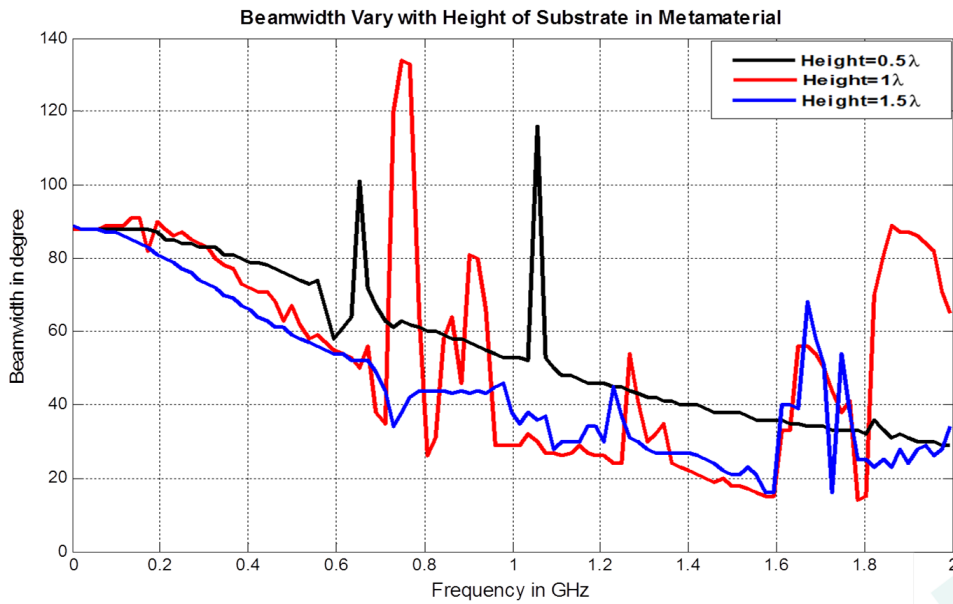


Figure 3.12: Beam width pattern plot for a metamaterial slot antenna with different substrate thickness, other constant values are:  $f_p=f_o=1\text{GHz}$ ,  $SL=2\lambda_p$ ,  $SW=0.125\lambda_p$ ,  $h=0.5\lambda_p$ ,  $1\lambda_p$ ,  $1.5\lambda_p$  and  $\text{Spacing}=0.5\lambda_p$

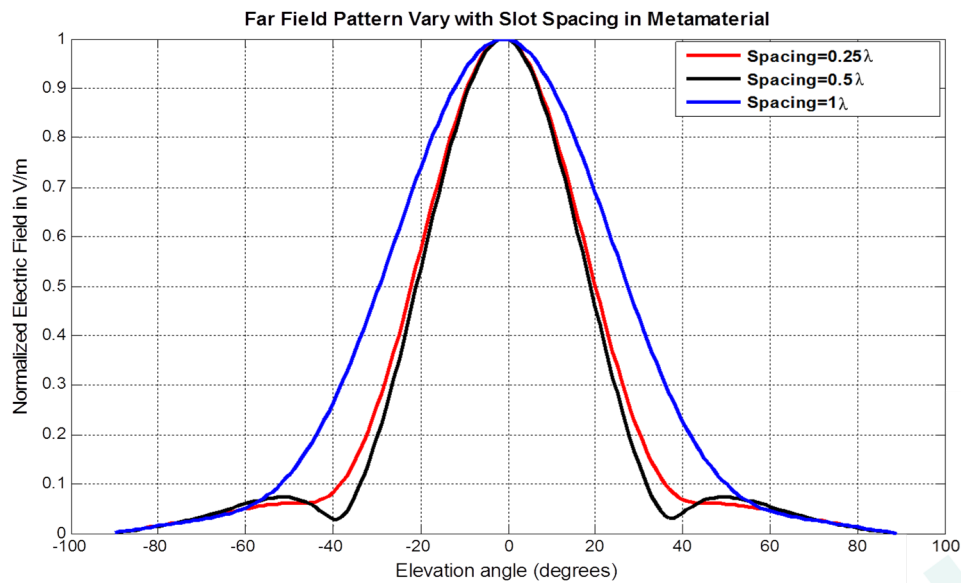
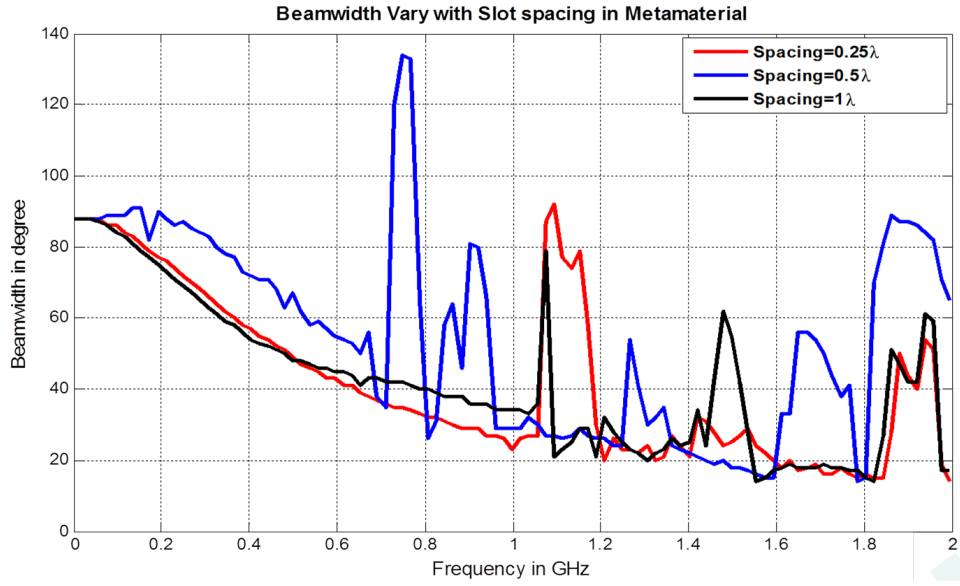


Figure 3.13: Normalized far field pattern plot for a metamaterial slot antenna with different slot spacing, other constant values are:  $f_p=f_o=1\text{GHz}$ ,  $SL=2\lambda_p$ ,  $SW=0.125\lambda_p$ ,  $h=1\lambda_p$  and  $\text{Spacing}=0.25\lambda_p$ ,  $0.5\lambda_p$  and  $1\lambda_p$



**Figure 3.14: Beam width pattern plot for a metamaterial slot antenna with different slot spacing, other constant values are:  $f_p=f_o=1\text{GHz}$ ,  $SL=2\lambda_p$ ,  $SW=0.125\lambda_p$ ,  $h=1\lambda_p$  and Spacing= $0.25\lambda_p$ ,  $0.5\lambda_p$  and  $1\lambda_p$**

slot length, slot width, slot spacing, distance between slots and thickness of substrate constant:  $f_o=f_p=1\text{GHz}$ ,  $SL=2\lambda_p$ ,  $SW=0.125\lambda_p$ , Spacing= $0.5\lambda_p$  and  $h=1\lambda_p$ . It is observed in Figure 3.15 that the directivity improves with the increase in the angle  $\phi$  from  $0^\circ$  to  $90^\circ$  in case of free space substrate, while in the metamaterial substrate medium the directivity increases for the decreasing azimuth angle  $\phi$  from  $90^\circ$  to  $0^\circ$ .

### 3.2.7 Case (VII)

In this case, we consider the variation of the normalized far field pattern or directivity and beam steering property of 3D two-slot antenna with the position of the source shifted towards either of the slot (left slot or right slot) along the x-axis, while keeping the slot length, slot width and thickness of substrate constant:  $f_o=f_p=1\text{GHz}$ ,  $SL=2\lambda_p$ ,  $SW=0.125\lambda_p$ , Spacing= $0.5\lambda_p$  and  $h=1\lambda_p$ . It is observed in Figure 3.16 for freespace and Figure 3.17 for metamaterial substrate medium that the beam steering effect is seen, as the far-field radiation pattern gets shifted towards the left when the source is moved along the negative X-axis, both in case of freespace and metamaterial medium.

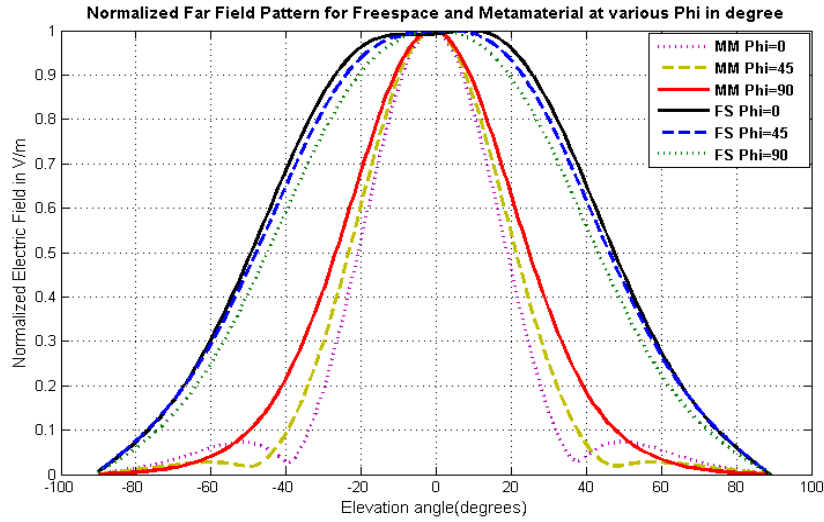


Figure 3.15: Normalized far field pattern plot for free space and metamaterial substrate medium with different phi angle, other constant values are:  $f_p=f_o=1\text{GHz}$ ,  $SL=2\lambda_p$ ,  $SW=0.125\lambda_p$ ,  $h=1\lambda_p$  and  $\text{Spacing}=0.5\lambda_p$

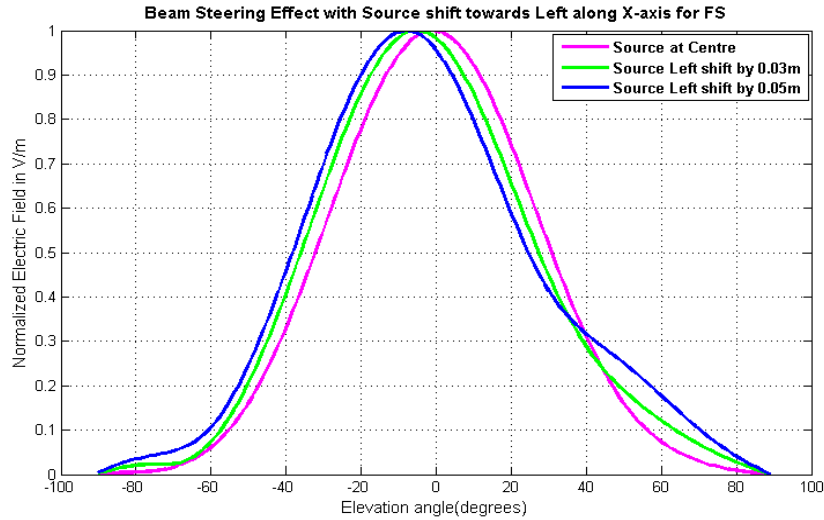
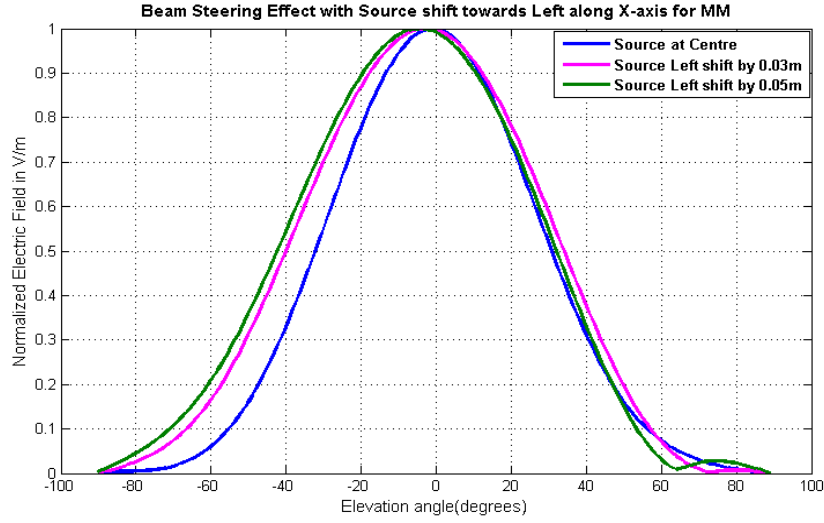


Figure 3.16: Normalized far field pattern plot for different position of source shift towards the left along the X-axis for Freespace medium, other constant values are:  $f_p=f_o=1\text{GHz}$ ,  $SL=2\lambda_p$ ,  $SW=0.125\lambda_p$ ,  $h=1\lambda_p$  and  $\text{Spacing}=0.5\lambda_p$



**Figure 3.17: Normalized far field pattern plot for different position of source shift towards the left along the X-axis for Metamaterial medium, other constant values are:  $f_p=f_o=1\text{GHz}$ ,  $SL=2\lambda_p$ ,  $SW=0.125\lambda_p$ ,  $h=1\lambda_p$  and  $\text{Spacing}=0.5\lambda_p$**

### 3.2.8 Case (VIII)

In this case, we consider the variation of the normalized far field pattern or directivity and beam steering property of 3D two-slot antenna with the position of source towards the length of the slot along the z-axis, while keeping the slot length, slot width and thickness of substrate constant:  $f_o=f_p=1\text{GHz}$ ,  $SL=2\lambda_p$ ,  $SW=0.125\lambda_p$ ,  $\text{Spacing}=0.5\lambda_p$  and  $h=1\lambda_p$ . It is observed in Figure 3.18 for the freespace medium and Figure 3.19 for the metamaterial medium that there is approximately zero phase shift or no beam steering effect when the source is moved along the Z-axis, as the far-field plot shows no shift w.r.t the centre position at elevation angle  $\theta=0^\circ$ .

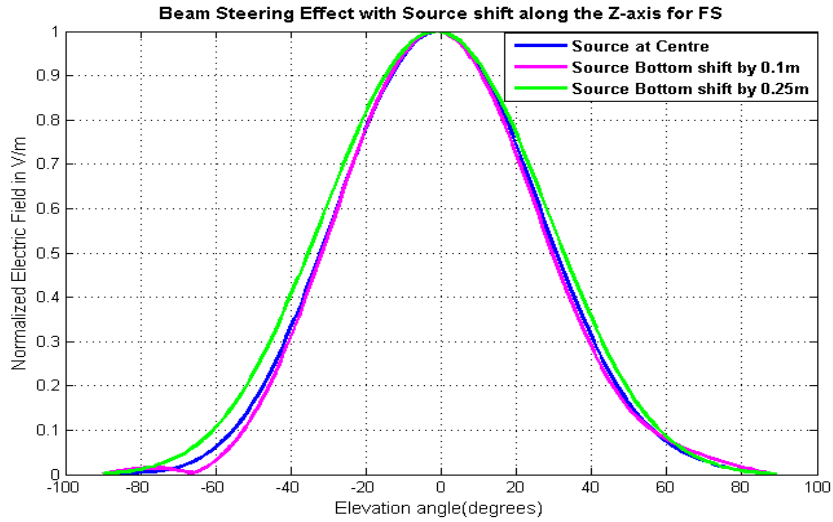


Figure 3.18: Normalized far field pattern plot for different position of source shift towards the bottom along the Z-axis for Freespace medium, other constant values are:  $f_p=f_o=1\text{GHz}$ ,  $SL=2\lambda_p$ ,  $SW=0.125\lambda_p$ ,  $h=1\lambda_p$  and  $\text{Spacing}=0.5\lambda_p$

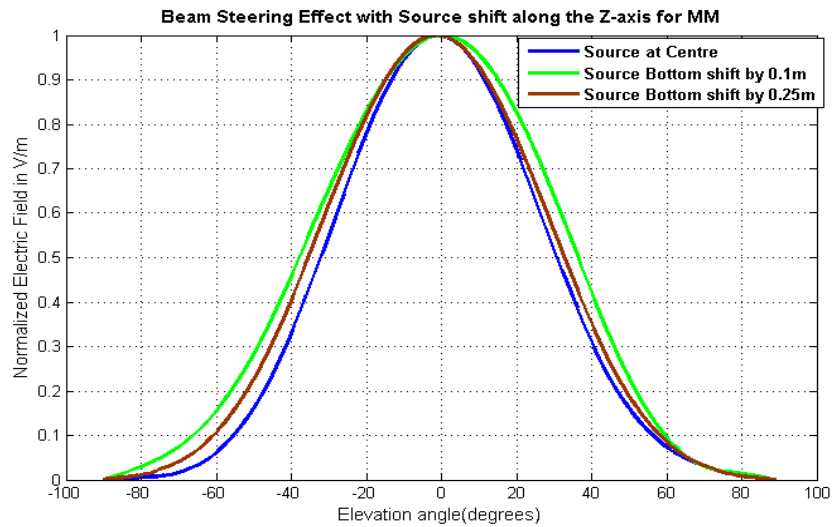


Figure 3.19: Normalized far field pattern plot for different position of source shift towards the bottom along the Z-axis for Metamaterial medium, other constant values are:  $f_p=f_o=1\text{GHz}$ ,  $SL=2\lambda_p$ ,  $SW=0.125\lambda_p$ ,  $h=1\lambda_p$  and  $\text{Spacing}=0.5\lambda_p$

**Table 3.1: Summary of our studies based on the various cases described**

Taking constant: Slotwidth  $SW=0.125\lambda_p$ , Spacing= $0.5\lambda_p$ , FS=Freespace, MM=Metamaterial

Case	Plasma frequency, $f_p$	Slot length, SL	Thickness, h	Inferences
Case I	1 GHz MM compared with FS substrate medium	$2\lambda_p$	$1\lambda_p$	Improvement in beam width is achieved by $35^\circ$ .
Case I	$f_o \neq f_p$	$2\lambda_p$	$1\lambda_p$	With change in $\omega_o$ beam width or directivity improves for $f_o=f_p=1\text{GHz}$ . Low beam width for $L=2, 2.5$ and $3$ but almost same.
Case II	1 GHz	Varying	$1\lambda_p$	Tradeoff between beam width and bandwidth of frequency.
Case III	1 GHz	$2\lambda_p$	$1\lambda_p$	Directivity remains constant with varying slot width.
Case IV	1 GHz	$2\lambda_p$	Varying	Beam width converges for $T=1$ and $T=1.5$ . Higher bandwidth for $T=1$ .
Case V	1 GHz	$2\lambda_p$	$1\lambda_p$	Directivity remains constant with varying slot spacing within $0.5\lambda$ .

## Chapter 4

# Conclusion and Future Work

### 4.1 Conclusion

A three dimensional (3D) slot antenna with a metamaterial substrate is simulated using FDTD techniques and the far field radiation and beam width patterns are generated. The behavior of the antenna for different parameters such as the length of the slot, width of the slot, the height of the substrate, spacing between the slots, position of the source and the plasma frequency of the substrate, is analyzed. The various key findings we achieved are:

1. The directivity of the 3D two-slot antenna with a metamaterial substrate was found to substantially improve upon the directivity of a conventional slot antenna with air substrate. Furthermore, the improved directivity was achieved for a bandwidth of frequencies around the plasma frequency.
2. As the size of the aperture (slot length) increases, the directivity of the antenna also increases till it converges, while as the slot width increases, the directivity of antenna remains almost constant. However, there is a tradeoff between beam width and bandwidth of the antenna.
3. As the height of the substrate increases, the directivity increases till it reaches convergence.
4. The choice of the distance between the two slots of the metamaterial substrate 3D two-slot antenna impacts the directivity in accordance with the array factor theory which implies that within the distance between the slots to be  $0.5\lambda$  the directivity remains almost constant, while when we increase the spacing beyond  $\lambda$  the grating lobes start getting formed and reduce the directivity of the far-field pattern.

5. Directive emission, away from the broadside is achieved using a two-slot array antenna with a near zero refractive index (NZI) substrate enclosing the Gaussian source.
6. The electronic beam scanning is thus achieved by the two-slot array antenna by varying the position of the source (centre and towards either of the two slots) along the x-axis (axis of array elements), however, the variation of the position of source along the z-axis (orientation direction of the slots) has no impact.

## 4.2 Future Work

1. We have analysed the radiation behaviour of a 3D two-slot array antenna element; this study could easily be extended to a multi-slot antenna array with a metamaterial substrate along the lines of a leaky wave antenna. Array parameters such as spacing between the elements, differential phasing of the elements, source excitation phase etc. could be studied to further improve the performance of the antenna. The 3D modeling would result in a more realistic simulation of practical antenna array implementations.

2. The analysis, computation and simulation of the effect of metamaterial substrate on the Doppler shift when the source is placed inside the substrate while the target is placed in the free space region structure could be done.

Finally, our proposed 3D antenna array design can be validated with measurement data collection with an actual hardware implementation. The plasma behaviour of the substrate can be achieved with split ring resonators and thin metal wires periodically arranged.

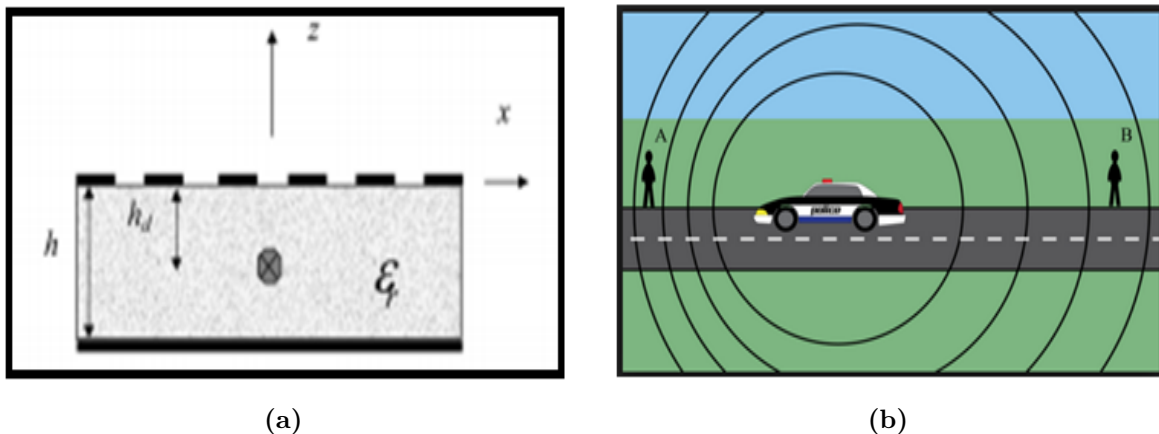


Figure 4.1: (a) Side-view of multi-slot antenna array structure (b) Doppler Shift

# Bibliography

- [1] BACCARELLI, P., BURGHIGNOLI, P., FREZZA, F., GALLI, A., LAMPARIELLO, P., LOVAT, G., AND PAULOTTO, S. Effects of leaky-wave propagation in metamaterial grounded slabs excited by a dipole source. *Microwave Theory and Techniques, IEEE Transactions on* 53, 1 (2005), 32–44.
- [2] BERENGER, J.-P. A perfectly matched layer for the absorption of electromagnetic waves. *Journal of computational physics* 114, 2 (1994), 185–200.
- [3] CALOZ, C., AND ITOH, T. *Electromagnetic metamaterials: transmission line theory and microwave applications*. John Wiley & Sons, 2005.
- [4] CALOZ, C., AND ITOH, T. Metamaterials for high-frequency electronics. *Proceedings of the IEEE* 93, 10 (2005), 1744–1752.
- [5] CHEEMA, H. M., AND SHAMIM, A. The last barrier. *IEEE Microwave Magazine* 14, 1 (2013), 79–91.
- [6] CORREIA, D., AND JIN, J. Theoretical analysis of left-handed metamaterials using fdtd-pml method. In *Microwave and Optoelectronics Conference, 2003. IMOC 2003. Proceedings of the 2003 SBMO/IEEE MTT-S International* (2003), vol. 2, IEEE, pp. 1033–1036.
- [7] ECE, I.-D. M. T. *Two Dimensional Metamaterial Slot Antenna for Improved Directivity*. PhD thesis, Indraprastha Institute of Information Technology New Delhi, 2014.
- [8] ENOCH, S., TAYEB, G., SABOUROUX, P., GUÉRIN, N., AND VINCENT, P. A metamaterial for directive emission. *Physical Review Letters* 89, 21 (2002), 213902.
- [9] HARRINGTON, R. F. *Time-harmonic electromagnetic fields*. McGraw-Hill, 1961.

- [10] KIM, D., KIM, N., CHEON, C., AND KWON, Y. A planar covered multi-slot-array heat applicator with beam scanning capability for interstitial microwave hyperthermia. In *Microwave Symposium Digest (MTT), 2010 IEEE MTT-S International* (2010), IEEE, pp. 1608–1611.
- [11] KIM, S.-H. Reference manual for pfdtd ver. 8.47.
- [12] LIU, H., FAN, Y., ZHOU, K., LI, L., AND SHI, X. High-directivity antenna using reconfigurable near-zero index metamaterial superstrates. In *Antennas and Propagation Society International Symposium (APSURSI), 2014 IEEE* (2014), IEEE, pp. 1546–1547.
- [13] LOVAT, G., BURGHIGNOLI, P., CAPOLINO, F., JACKSON, D. R., AND WILTON, D. R. Analysis of directive radiation from a line source in a metamaterial slab with low permittivity. *Antennas and Propagation, IEEE Transactions on* 54, 3 (2006), 1017–1030.
- [14] SCHELKUNOFF, S. Some equivalence theorems of electromagnetics and their application to radiation problems. *Bell System Technical Journal* 15, 1 (1936), 92–112.
- [15] SULLIVAN, D. M. Frequency-dependent fdtd methods using z transforms. *Antennas and Propagation, IEEE Transactions on* 40, 10 (1992), 1223–1230.
- [16] SULLIVAN, D. M. A simplified pml for use with the fdtd method. *Microwave and Guided Wave Letters, IEEE* 6, 2 (1996), 97.
- [17] SULLIVAN, D. M. *Electromagnetic simulation using the FDTD method*. John Wiley & Sons, 2013.
- [18] VESELAGO, V. G. The electrodynamics of substances with simultaneously negative values of  $\epsilon$  and  $\mu$ . *Physics-Uspokhi* 10, 4 (1968), 509–514.
- [19] WENG, Z.-B., WANG, N.-B., AND JIAO, Y.-C. Study on high gain patch antenna with metamaterial cover. In *2006 7th International Symposium on Antennas, Propagation & EM Theory* (2006), pp. 1–2.
- [20] ZHOU, R., ZHANG, H., AND XIN, H. Metallic wire array as low-effective index of refraction medium for directive antenna application. *Antennas and Propagation, IEEE Transactions on* 58, 1 (2010), 79–87.

- [21] ZIOLKOWSKI, R. W. Propagation in and scattering from a matched metamaterial having a zero index of refraction. *Physical Review E* 70, 4 (2004), 046608.
- [22] ZIOLKOWSKI, R. W., AND HEYMAN, E. Wave propagation in media having negative permittivity and permeability. *Physical review E* 64, 5 (2001), 056625.

## List of Publications

1. “*Multiple Slot Array with Near Zero Refractive Index Substrate*”, authors, Namrata Singh and Shobha Sundar Ram, accepted in Antennas and Propagation Society International Symposium (APS/URSI), Vancouver, Canada, July, 2015.